Shortest Paths for Finned, Winged, Legged and Wheeled Vehicles with Side–Looking Sensors*

Paolo Salaris,† Lucia Pallottino,† Antonio Bicchi†‡

Abstract

Sensor-guided robotic locomotion in different media often takes inspiration from natural examples, e.g. from fishes, birds, and humans for underwater, aerial, or walking robots, respectively. Interestingly, several naturalistic observations show that even very different species exhibit some similarities in their locomotion patterns: a notable one perhaps being the spiraling nature of paths that in some cases can be observed in sensory-guided tasks. As often conjectured in naturalistic studies, a common optimality principle may underpin such motion behaviors. We show in a robotics framework that spiraling motions appear in the solution of the problem of minimum path length. In particular, we study optimal paths for a simple model of finned, winged, and legged robotic vehicles, under different constraints on the field-of-view of the available sensory inputs. After showing that logarithmic spirals are indeed extremals of a sensory-constrained shortest path problem, we provide a complete synthesis of the optimal control for different robotic vehicles. Applications of these results to robotics can reduce the length of paths to be followed by underwater, aerial or legged robots to reach targets in their environment. The work also provides some interesting, although preliminary, insights into how sensory field-of-view limitations may influence motion patterns in natural systems.

1 Introduction

Biological observations show that many different species in nature, including fishes, birds, and humans, exhibit surprisingly similar behaviours in their locomotion. Indeed, it has been known for long time ([Lyon, 1899; Schaeffer, 1920]) that in the locomotion of animals it is possible to discern the presence of spiralling components. This

*This work was supported by E.C. contracts n.224053 CONET (Cooperating Objects Network of Excellence), n. 257462 HYCON2 (Network of Excellence) and n.2577649 PLANET. This paper extends and improves the work in [Salaris et al., 2011] where, for space limitation, several proofs and technical details have been omitted, especially for particular sensor configurations.

†The Interdept. Research Center "Enrico Piaggio", University of Pisa, via Diotisalvi 2, 56100 Pisa, Italy. paolo.salaris,l.pallottino,bicchi@centropiaggio.unipi.it

‡Department of Advanced Robotics, Istituto Italiano di Tecnologia, via Morego, 30, 16163 Genova, Italy

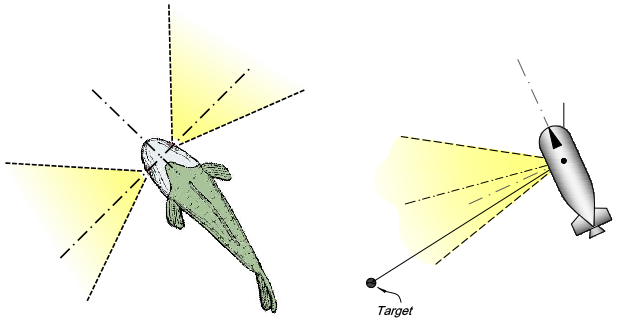

(a) Nurse shark and goldfish vision system.

(b) Underwater (Finned) vehicle with lateral-looking sensors.

Figure 1: Fish vision system and lateral sensors.

has been observed in a range of organisms going from the simplest unicellular organisms ([Bullington, 1925]) to mammals ([Dunkelberger, 1926]) and humans ([Schaeffer, 1928]). For example, in [Kleerekoper et al., 1973] a study of the locomotor patterns of nurse sharks indicated that the approach by these animals to a source of diffusing odor or light was along *logarithmic spirals*, i.e. equiangular spirals in which the lengths of radii at 90^o are in the golden ratio $\Phi = \frac{1-\sqrt{5}}{2}$, (see figure 1). Authors of [Kleerekoper et al., 1973] state that "bilateral sense organs may play a role in steering logarithmic spiral movements", although evidence is inconclusive as to which "the mechanisms by which spiral movements are brought about" are. A conclusion that laterality of sense organs (both visual and olfactory) and the limited aperture of their receptive fields determine logarithmic spiral movements is not warranted by experimental observations: indeed, e.g. goldfishes continue moving in spirals even when blinded ([Kleerekoper et al., 1973]). However, the same authors conclude that "the significance of logarithmic spiralling in directed locomotion toward a stimulus source gains importance" in relation to a model (credited to F. Brouwer in [Kleerekoper et al., 1973]), which states that "any target–seeking device which approaches the target in a direct pathway which, at all times, deviates with a constant angle from a straight line connecting the vehicle with the target, will describe a logarithmic spiral around the target."

Similarly, spiral paths have been observed in flying animals orienting themselves with respect to a light source [Fraenkel and Gunn, 1961]. For example, several insects with compound eyes consisting of many ommatidia (single-axon light detectors) have been observed to fly trajectories such that the same group of ommatidia remain activated, which requires keeping a constant angle between the forward direction and the beams of light. This behaviour serves the purpose of following straight paths whenever the light source is far enough that the light beams are parallel, as e.g. when using the sun or the moon for orientation. However, when the light source is close, a logarithmic spiral towards the source results, as confirmed e.g. by observations of moth flight (see [Boyadzhiev, 1999]). Fundamentally the same behaviour can be observed in raptors during hunting activities ([Tucker, 2000], reported already in [Salaris et al., 2010]). As

raptors possess no accurate front sight, to approach a prey at high velocity they dive along a logarithmic spiral with their head straight and one eye looking sideway at the prey, rather than following the straight path to the prey with their head inefficiently turned sideways (see figure 2).

Human locomotion and the optimizing principles underlying the shape of trajectories performed have been studied again recently with a more analytical approach. In [Arechavaleta et al., 2008b], authors show the directional nature of human locomotion by analyzing trajectories recorded in 7 subjects during walking tasks in an empty space toward a goal defined both in position and orientation. However, in [Arechavaleta et al., 2008a], experimental results show that the subject's head points most of the time toward the target, thus suggesting a role of the limited field-of-view on the shape of the trajectories (see figure 3). Subsequently, in [Mombaur et al., 2010] authors present a more refined inverse optimal control approach to understand the cost functional that humans minimize during a rest-to-rest task, and eventually transfer biological motions to robots. An objective function was considered consisting in a weighted sum of five terms depending on the total time, the forward, angular and lateral acceleration components, and the bearing angle, respectively. Based on experimental data, authors calculated the best-fitting weights, and showed that the locomotion behavior corresponded to minimizing a cost functional in which the bearing angle weight is largest (optimal weights for the five terms were $(1, 1.2, 1.7, 0.7, 5.2)$, respectively). This observation is suggestive that results on shortest paths with limited FOV may provide relevant and interesting insight also in human locomotion.

Moving on to consider robotic applications, autonomous vehicles of different kinds often share two important characteristics with their natural counterpart, i.e. directionality of motion and limitation (and often laterality) of sensory Field–Of–View (FOV). These characteristics deeply influence the accomplishment of assigned tasks, which often imply that some environment objects or landmarks are kept in sight — be it for localization or tracking.

For example, many Autonomous Underwater Vehicles (AUV) used in underwater surveying and navigation are designed with a preferential direction of motion (the fore) to reduce drag, and are equipped with sonar scanners to detect and recognize objects (e.g. mines, wrecks, archeological findings) on the sea bed. Three types of sonars are usually used ([Hayes and Gough, 2009]): forward ([Jean, 2008]), side–looking ([Langner et al., 2009]), and squint ([Caprais and Guyonic, 1997]) sonars, differing for the angle between the vehicle heading and the main axis of the scanner beam. Sonars are used for mapping the sea bed for a wide variety of purposes, including creation of nautical charts and detection and identification of underwater objects and bathymetric features. Once salient features of the sea bed are observed, in order to reach, localize and/or recognize them, AUVs are required to move keeping them inside the limited FOV of the scanner.

Furthermore, an ever increasing number of wheeled (or tracked) ground vehicles use visual–based control. These vehicles, which are also steered about their preferential motion direction (perpendicular to the wheel axis), are often equipped with on-board monocular camera(s) with limited FOV. Again here the problem is to maintain in the features sight. This is necessary e.g. for visual servoing during robot trajectories: the problem is mentioned for instance in [Mariottini et al., 2007] and in [López-Nicolás

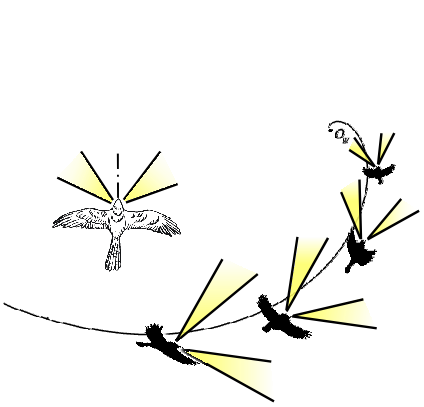

(a) Raptor vision system and trajectories followed to approach a prey.

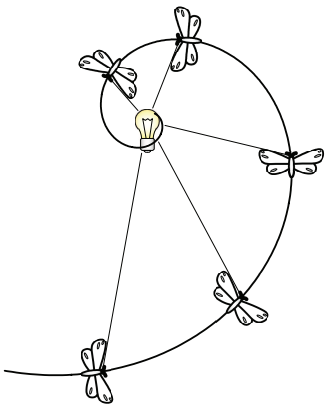

(b) Trajectories followed by moths to approach an electric light.

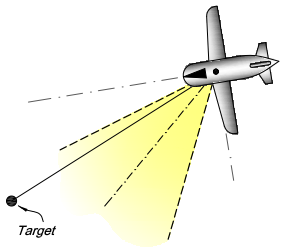

(c) Winged vehicle with side-looking sensors.

Figure 2: Raptor's trajectories during hunting activity and Side–looking sensors.

et al., 2008], although proposed solutions are valid only under rather favorable assumptions. FOV constraints are explicitly taken into account for the parking problem for a unicycle–like vehicle in [Murrieri et al., 2004], [Gans and Hutchinson, 2007b], and [Gans and Hutchinson, 2007a], and for a rendez-vous problem in [Yu et al., 2011]. However, the resultant path is not optimal, and indeed far from efficient. Although in many robotic applications cameras are mounted in front of the vehicle and point forward in the direction of motion, lateral sensing is sometimes used. In [Kawano et al., 2009] authors propose a vehicle equipped with side–looking camera for more effective generation of panoramic images of building walls. In [Li and Shimomura, 2008] a fisheye camera is mounted on the side of a vehicle in order to detect lane markings, thus avoiding occlusions due to other vehicles proceeding in front, a typical drawback of frontal and omnidirectional cameras mounted on top of the vehicle.

Regarding optimal (shortest) paths in absence of sensor constraints, the seminal work on unicycle vehicles, [Dubins, 1957], provides a characterization of shortest curves for a car with a bounded turning radius. In [Bui et al., 1994], authors determine a complete finite partition of the motion plane in regions characterizing the shortest path from all points in the same region, i.e. a synthesis. A similar problem with the

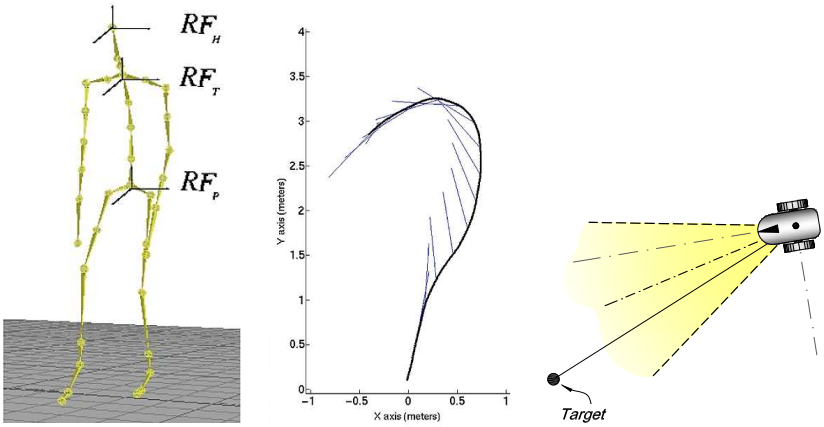

(a) Human reference frames (see [Arechavaleta et al., 2008a]).

(b) Human trajectories and head direction (see [Arechavaleta et al., 2008a]).

(c) Wheeled (or Legged) robot with Asymmetric Frontal sensors.

Figure 3: Human locomotion and Asymmetric Frontal sensors.

car moving both forward and backward has been solved in [Reeds and Shepp, 1990] and refined in [Sussmann and Tang, 1991]. The global synthesis for the Reeds and Shepp vehicle has been obtained combining necessary conditions given by Pontryagin's Maximum Principle (PMP) with Lie algebraic tools in [Souères and Laumond, 1996]. More recently, [Balkcom and Mason, 2006], [Wang et al., 2009] determined time optimal trajectories for differential–drive robots and nonholonomic bidirectional robots, respectively, while [Chitsaz et al., 2009] solved the minimum wheel rotation problem for differential-drive robots.

The optimal pursuit of targets taking into account limited sensor aperture is a classical problem in the field of guidance and control of aircrafts. For example, in [Salama and Hamza, 1978] an analysis to determine the optimal trajectories in three dimensional space for a point mass pursuer is performed. The study of various cases shows that in general the optimum trajectory consists of spirals and straight lines and lies in a single plane. More recently, in intelligence, reconnaissance, and surveillance missions, Unmanned Aerial Vehicles (UAVs) equipped with limited electro-optical and infrared cameras are used. These vehicles which have a preferential motion direction, are capable of surveying the environment in order to localize a target, providing the operator with real–time visual information rapidly and inexpensive. The main challenging in target localization include maintaining the target in the limited field–of–view and developing a UAV trajectory such that the target localization error is minimized ([Rysdyk, 2003; Ponda et al., 2009]). As for previous applications, the visibility limitations depend also on the way the camera is mounted on-board the UAVs ([Theodorakopoulos and Lacroix, 2008]).

Motivated by these robotic applications and biological inspirations, in this paper

we propose a systematic study of optimal (shortest) paths for a vehicle moving in a plane with a preferential direction of motion, to reach a target position while making sure that a single given landmark fixed in the plane is kept inside a limited FOV sensor modeled as a planar cone moving with the robot. After showing that logarithmic spirals are indeed extremals of a sensory-constrained shortest path problem, we provide (under some simplifying assumptions) a complete optimal synthesis for the considered problem, i.e. a finite language of optimal control words, and a global partition of the motion plane induced by shortest paths, such that a word in the optimal language is univocally associated to a region and completely describes the constrained shortest path from any starting point in that region to the goal point. Regions and associated optimal control words are at most 15, and the number depends on the sensor orientation with respect to the forward direction.

A first step toward the optimal solution of this problem has been done in [Bhattacharya et al., 2007] where a local shortest path synthesis has been provided for frontal FOV (i.e. the robot forward direction is included in the sensor cone, not necessarily symmetric). In [Salaris et al., 2010], a global shortest path synthesis was found for frontal and symmetric FOV. However, for lateral sensor systems, like in the fish or AUV examples, the forward direction of motion is not included in the FOV. For side sensor systems, like in the raptor or UAV examples, neither the forward direction nor its perpendicular lie inside the FOV. In this paper, we present a synthesis of shortest paths, which includes as particular solutions both the earlier results of [Bhattacharya et al., 2007] (within their local validity limitations) and of [Salaris et al., 2010], but generalizes upon those and provides a global solution for generic FOVs, including side and lateral sensors.

The impracticality of paths that point straight to the feature leads to a substantially more complex analysis of the reduction to a finite and sufficient family of optimal paths with respect to previous work. Furthermore, all the symmetries that characterized the symmetric and frontal FOV do not hold, and results in [Salaris et al., 2010] simply do not apply. For example, while studying optimal paths in the upper half of the motion plane was sufficient in [Salaris et al., 2010], the study here requires analyzing the full plane.

Applications of these results to robotics can reduce the length of paths to be followed by underwater, aerial or legged robots to reach targets in their environment. However, this work also provides an interesting, although preliminary, insight into how limited sensory FOV may influence motion patterns in natural systems.

2 Problem Definition

Consider a body moving on a plane and a right-handed reference frame $\langle W \rangle$ with origin in O_w and axes X_w, Z_w. The configuration of the moving body (hereafter referred to as "vehicle") is described by $\xi(t) = (x(t), z(t), \theta(t))$, where $(x(t), z(t))$ is the position in $\langle W \rangle$ of the reference central point in the vehicle, and $\theta(t)$ is the vehicle heading with respect to the X_w axis (see figure 4). The forward and angular velocities, $v(t)$ and $\omega(t)$ respectively, are the control inputs to the kinematic model (we assume that the dynamics are negligible). Choosing polar coordinates for the vehicle $\eta = [\rho\ \psi\ \beta]^T$

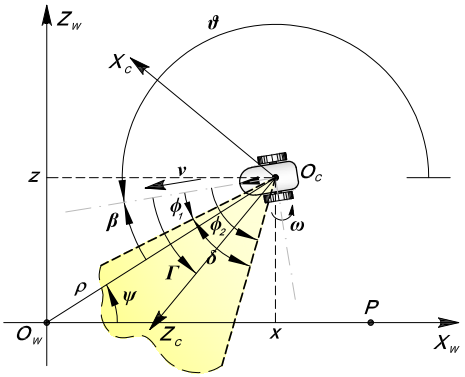

Figure 4: Autonomous vehicle and systems coordinates. The vehicle's task is to reach P while keeping O_w within a limited sensor range modeled as a planar cone (highlighted in color).

(see figure 4), the assumed kinematic model is therefore

$$\begin{bmatrix} \dot{\rho} \\ \dot{\psi} \\ \dot{\beta} \end{bmatrix} = \begin{bmatrix} -\cos\beta & 0 \\ \frac{\sin\beta}{\rho} & 0 \\ \frac{\sin\beta}{\rho} & -1 \end{bmatrix} \begin{bmatrix} v \\ \omega \end{bmatrix}. \tag{1}$$

We consider vehicles with bounded velocities which can turn on the spot. In other words, we assume

$$(v, \omega) \in U, \tag{2}$$

with U a compact and convex subset of $\mathbb{R}^2$, containing the origin in its interior.

The vehicle is equipped with a rigidly fixed sensor system with a reference frame $\langle C \rangle = \{O_c, X_c, Y_c, Z_c\}$. The center O_c corresponds to the robot's center $[x(t), z(t)]^T$ and the forward sensor axis Z_c forms an angle Γ w.r.t. the robot's forward direction. Moreover, let δ be the characteristic angle of the cone characterizing the limited Field–Of–View (FOV) and let us consider the most interesting problem in which $\delta \leq \pi/2$. Without loss of generality, we will assume $0 \leq \Gamma \leq \frac{\pi}{2}$, so that, when $\Gamma = 0$ the Z_c axis is aligned with the robot's forward direction (i.e. the particular case solved in [Salaris et al., 2010]), whereas, when $\Gamma = \frac{\pi}{2}$, the Z_c axis is perpendicular to the robot's forward direction. Consider $\phi_1 = \Gamma - \frac{\delta}{2}$ and $\phi_2 = \Gamma + \frac{\delta}{2}$ the angles between the robot's forward direction and the right or left sensor's border w.r.t. Z_c axis, respectively. The restriction on $0 \leq \Gamma = \frac{\phi_1 + \phi_2}{2} \leq \frac{\pi}{2}$ will be removed at the end of this paper, where an easy procedure to obtain the synthesis for any value of Γ will be given.

We also assume that the feature to be kept within the FOV is placed on the axis through the origin O_w and perpendicular to the plane of motion. Moreover, the position of the robot target point P is on the X_w axis, with coordinates $(\rho, \psi) = (\rho_P, 0)$.

The planar FOV, with characteristic angle $\delta = |\phi_2 - \phi_1|$, generates the following

constraints:

$$\beta - \phi_1 \geq 0\,, \tag{3}$$
$$\beta - \phi_2 \leq 0\,. \tag{4}$$

Note that we place no restrictions on the vertical dimension of the sensor. Therefore, the height of the feature on the motion plane, which corresponds to its Y_c coordinate in the sensor frame $\langle C \rangle$, is irrelevant to our problem. Hence, for our purposes, it is necessary to know only the projection of the feature on the motion plane, i.e. O_w.

The goal of this paper is to determine, for any point $Q \in \mathbb{R}^2$ in the robot space, the shortest path from Q to P such that the feature in O_w is maintained in the FOV of the sensor. In other words, we want to minimize the length of the path covered by the center of the vehicle under the *feasibility constraints* (1), (2), (3), and (4).

From the theory of optimal control with state and control constraints and Pontryagin Maximum Principle (PMP) (see [Pontryagin et al., 1962], [Bryson and Ho, 1975]) it is possible to show that, when constraints (3) and (4) are not active, extremal curves (i.e. curves that satisfy necessary conditions for optimality), are straight lines (denoted as S) and rotations on the spot (denoted as $*$). On the other hand, when constraints (3) and (4) are active, necessary conditions for optimality imply

$$\begin{aligned} \beta - \phi_1 \equiv 0 \qquad &\Rightarrow \qquad \tan\beta = \tan\phi_1 \\ \beta - \phi_2 \equiv 0 \qquad &\Rightarrow \qquad \tan\beta = \tan\phi_2\,, \end{aligned}$$

and, by (1),

$$\dot{\psi} \;=\; \tan\phi\frac{\dot{\rho}}{\rho} = -\tan\phi_1\frac{d}{dt}(\ln\rho)\,, \text{ when } \beta = \phi_1 \tag{5}$$
$$\dot{\psi} \;=\; \tan\phi_2\frac{\dot{\rho}}{\rho} = -\tan\phi_2\frac{d}{dt}(\ln\rho)\,, \text{ when } \beta = \phi_2\,. \tag{6}$$

Integrating, we obtain

$$\psi \;=\; \tan\phi_1 \ln\left(\frac{\rho}{\rho_o}\right), \text{ when } \beta = \phi_1\,, \tag{7}$$
$$\psi \;=\; \tan\phi_2 \ln\left(\frac{\rho}{\rho_o}\right), \text{ when } \beta = \phi_2\,, \tag{8}$$

where ρ_o is a constant that depends on initial conditions.
Equations (7) and (8) represent two logarithmic spirals with characteristic angle ϕ_1 and ϕ_2, respectively, rotating around the landmark located in O_w. Logarithmic spirals with characteristic angle $\phi_i > 0$ rotate counterclockwise around O_w, whereas with $\phi_i < 0$ they rotate clockwise around O_w. We refer to these two kind of spirals as *Left* and *Right* and by symbols T_i^L and T_j^R with $i, j \in \{1,2\}$. The adjectives "Left" and "Right" indicate the half-plane where the spiral starts for an on-board observer aiming at the landmark.

Notice that, for $\phi_2 = \pi/2$ the left sensor border is perpendicular to the robot's forward direction and by equation (8) we have $\rho = \rho_o$, and hence, the extremal arc is

a circle centered in O_w (denoted as C). For $\phi_1 = 0$ the right sensor border is aligned with the direction of motion, and hence when right sensor constraint is active we have $\beta = 0$: the extremal arc is an half–line through O_w (denoted as H). In other words, when $\phi_2 = \pi/2$ spiral T_2 degenerates in a circle centered in O_w, whereas when $\phi_1 = 0$ spiral T_1 degenerates in an half–line through O_w.

Extremal arcs can be executed by the vehicle in either forward ($v > 0$) or backward ($v < 0$) direction: we will hence use superscripts $+$ and $-$ to make this explicit (e.g. S^- stands for a straight line executed backward).

We will build extremal paths consisting of sequences of symbols, or *words*, in the alphabet $\mathscr{A} = \{*, S^+, S^-, E_1^+, E_1^-, E_2^+, E_2^-\}$, where the actual meaning of symbols depends on angles Γ and δ as in figure 5. Rotations on the spot ($*$) have zero length, but may be used to properly connect other maneuvers. In particular, figure 5(a) shows the *Frontal* case, i.e. with $0 < \Gamma < \frac{\delta}{2}$, figure 5(b) shows the *Borderline Frontal* case, i.e. with $\Gamma = \frac{\delta}{2}$, figure 5(c) shows the *Side* case, i.e. with $\frac{\delta}{2} < \Gamma < \frac{\pi-\delta}{2}$, figure 5(d) shows the *Borderline Side* case, i.e. with $\Gamma = \frac{\pi-\delta}{2}$, and, finally, figure 5(e) and figure 5(f) show the *Lateral and Symmetric Lateral* case, i.e. with $\frac{\pi-\delta}{2} < \Gamma < \frac{\pi}{2}$ and $\Gamma = \frac{\pi}{2}$, respectively.

No other information on how extremals must be combined in optimal paths can be obtained from the application of the PMP. Hence, the paper exploits physical and geometrical constraints of the considered problem to overcome this. Let $\mathscr{L}_\Gamma$ be the set of possible words generated by the aforementioned symbols in $\mathscr{A}$ for each value of Γ, the rest of the paper is dedicated to showing that a sufficient optimal finite language $\mathscr{L}_O \subset \mathscr{L}_\Gamma$ can be built such that, for any initial condition, it contains a word describing a path to the goal which is no longer than any other feasible path. Correspondingly, a partition of the plane in a finite number of regions is described, for which the shortest path is one of the words in $\mathscr{L}_O$.

3 Shortest path synthesis

In this section, we introduce the basic tools that will allow us to study the optimal synthesis of the whole state space of the robot, beginning from points on a particular subset of $\mathbb{R}^2$ such that the optimal paths are in a sufficient optimal finite language, i.e. a finite language that contains words representing paths that are no longer than any other feasible path. Based on the geometrical properties of extremals, we introduce the following map,

Definition 1. *Given the target point $P = (\rho_P, 0)$ in polar coordinates, and $Q \in \mathbb{R}^2 \setminus O_w$, $Q = (\rho_Q, \psi_Q)$ with $\rho_Q \neq 0$, let $f_Q : \mathbb{R}^2 \to \mathbb{R}^2$ denote the map*

$$f_Q(\rho_K, \psi_K) = \begin{cases} \left(\dfrac{\rho_K \rho_P}{\rho_Q}, \psi_K - \psi_Q\right) & \text{for } \rho_K \neq 0 \\ (0,0) & \text{otherwise.} \end{cases} \tag{9}$$

The map f_Q is the combination of a clockwise rotation by angle $\psi_K - \psi_Q$, and a scaling by a factor ρ_P/ρ_Q that maps Q in P.

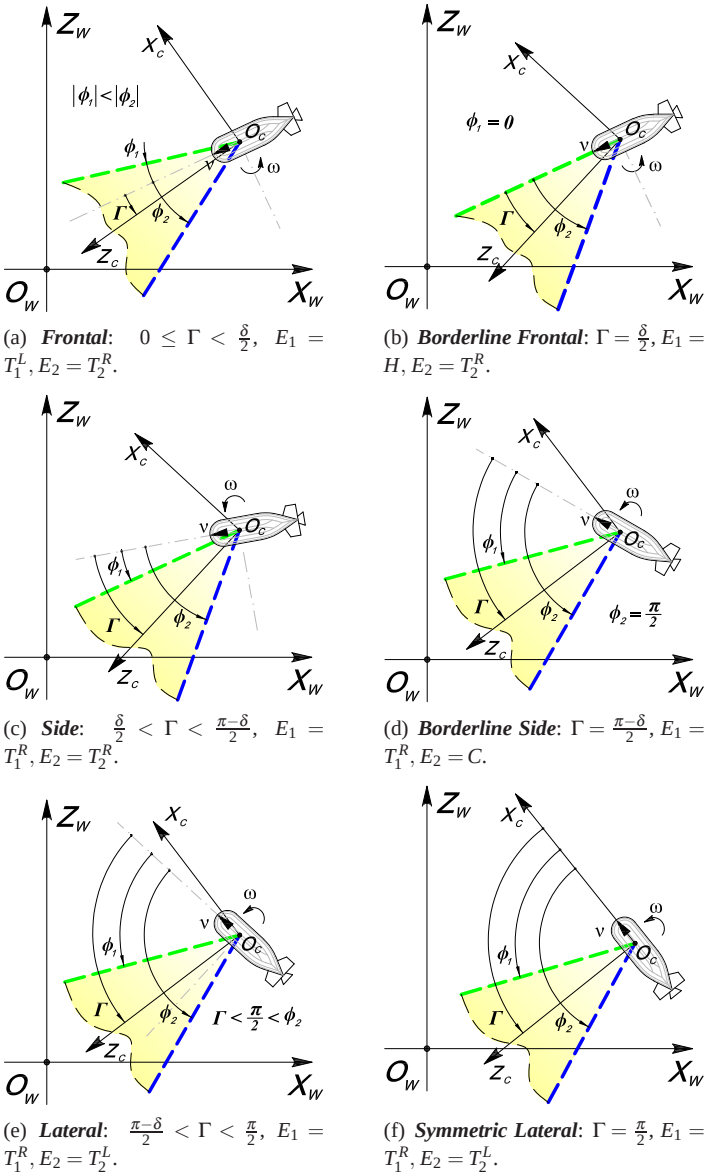

(a) ***Frontal***: $0 \leq \Gamma < \frac{\delta}{2}$, $E_1 = T_1^L, E_2 = T_2^R$.

(b) ***Borderline Frontal***: $\Gamma = \frac{\delta}{2}, E_1 = H, E_2 = T_2^R$.

(c) ***Side***: $\frac{\delta}{2} < \Gamma < \frac{\pi-\delta}{2}$, $E_1 = T_1^R, E_2 = T_2^R$.

(d) ***Borderline Side***: $\Gamma = \frac{\pi-\delta}{2}, E_1 = T_1^R, E_2 = C$.

(e) ***Lateral***: $\frac{\pi-\delta}{2} < \Gamma < \frac{\pi}{2}$, $E_1 = T_1^R, E_2 = T_2^L$.

(f) ***Symmetric Lateral***: $\Gamma = \frac{\pi}{2}, E_1 = T_1^R, E_2 = T_2^L$.

Figure 5: Sensor configuration depending on angles Γ and δ.

Remark 1. *The alphabet $\mathscr{A}$ is invariant w.r.t. rotation and scaling. However, it is not invariant w.r.t. axial symmetry, as it happened in the particular case (i.e. the Frontal case with $\Gamma = 0$) considered in [Salaris et al., 2010], where the map f_Q was defined as a combination of rotation, scaling and axial symmetry. For example, logarithmic spirals are self-similar and self-congruent (under scaling and rotation they are*

mapped into themselves). On the other hand, left (right) spirals are mapped into right (left) spirals through an axial symmetry and alphabet invariancy can be lost. Indeed, for example, considering the Side case alphabet (see figure 5(c)) $\mathscr{A}_{Side} = \{*, S^+, S^-, T_1^{R+}, T_1^{R-}, T_2^{R+}, T_2^{R-}\}$*, and applying an axial symmetry we have* $T_1^R \rightarrow T_1^L \notin \mathscr{A}_{Side}$*, the same occurs for the Frontal alphabet with* $\Gamma > 0$*.*

Based on f_Q, which maps points in points, we now introduce a new map F_Q sending paths in paths, which will be instrumental in reducing the search domain for optimal solutions. Let γ be a path parameterized by $t \in [0,1]$ in the plane of motion $\gamma(t) = (\rho(t), \psi(t))$. Denote with $\mathscr{P}_Q$ the set of all feasible extremal paths from $\gamma(0) = Q$ to $\gamma(1) = P$.

Definition 2. *Given the target point* $P = (\rho_P, 0)$ *and* $Q = (\rho_Q, \psi_Q)$ *with* $\rho_Q \neq 0$*, let the* path transform *function* F_Q *be defined as*

$$\begin{aligned} F_Q : \mathscr{P}_Q &\rightarrow \mathscr{P}_{f_Q(P)} \\ \gamma(t) &\mapsto f_Q(\gamma(1-t)), \forall t \in I. \end{aligned} \tag{10}$$

Notice that $\tilde{\gamma}(t) = F_Q(\gamma(1-t))$ corresponds to $\gamma(t)$ transformed by f_Q and followed in opposite direction. Indeed, $\tilde{\gamma}$ is a path from $\tilde{\gamma}(0) = f_Q(P) = \left(\frac{\rho_P^2}{\rho_Q}, -\psi_Q\right)$ to $\tilde{\gamma}(1) = f_Q(Q) \equiv P$.

We will denote the circle with center in O_w and radius ρ_P by $C(P)$ and the closed disk within $C(P)$ by $D(P)$. $C(P)$ has an important role in the proposed approach since properties of F_Q will allow us to solve the synthesis problem from points on $C(P)$, and hence to extend the synthesis to $D(P)$ and to the whole motion plane. Indeed, $\forall Q \in C(P)$ and $\forall \gamma \in \mathscr{P}_Q$, $F_Q(\gamma) \in \mathscr{P}_{f_Q(P)}$ with $f_Q(P) \in C(P)$, i.e. a path from a point $Q = (\rho_P, \psi_Q)$ on $C(P)$ to P is mapped in a path from point $f_Q(P) = (\rho_P, -\psi_Q)$ on $C(P)$ to P.

Furthermore, F_Q transforms an extremal in $\mathscr{A}$ in itself but followed in opposite direction. Hence, F_Q maps extremal paths in $\mathscr{L}_\Gamma$ in extremal paths in $\mathscr{L}_\Gamma$. For example, let $w = S^- * H^- * S^+ * T_2^{R+}$ be the word that characterize a path from Q to P, the transformed path is of type $z = T_2^{R-} * S^- * H^+ * S^+$. With a slight abuse of notation, we will write $z = F_Q(w)$.

Proposition 1. *Given* $Q \in \mathbb{R}^2$ *and a path* $\gamma \in \mathscr{P}_Q$ *of length* l*, the length of the transformed path* $\tilde{\gamma} = F_Q(\gamma)$ *is* $\tilde{l} = \frac{\rho_P}{\rho_Q} l$*.*

The proof is based on the fact that scaling transformation scales of the same quantity the lengths of both straight and spiral arcs. Indeed, the length d of a spiral arc between $A = (\rho_A, \psi_A)$ and $B = (\rho_B, \psi_B)$ is linear in ρ, i.e. $d = \frac{\rho_A - \rho_B}{\cos\phi}$, see [Salaris et al., 2010] for a formal proof.

Based on the properties of F_Q, optimal paths from points on $C(P)$ completely evolve inside $C(P)$. To prove this statement we first report the following result,

Theorem 1. *Given two points* $A = (\rho_A, \psi_A)$ *and* $B = (\rho_B, \psi_B)$*, with* $\psi_A > \psi_B$ *and* $\rho = \rho_A = \rho_B$*, and an extremal path* γ *from A to B such that for each point G of* γ*,* $\rho_G > \rho$*, there exists an extremal path* $\tilde{\gamma}$ *from A to B such that for each point* $\tilde{G}$ *of* $\tilde{\gamma}$*,* $\rho_{\tilde{G}} < \rho$ *and* $\ell(\tilde{\gamma}) < \ell(\gamma)$ *(see figure 6).*

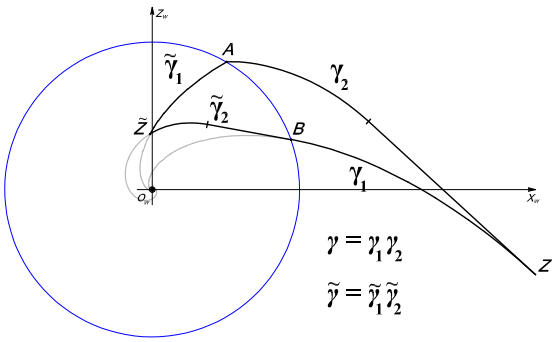

Figure 6: An example for theorem 1: path $\gamma = \gamma_2\gamma_1$ (γ_2 followed by γ_1) of type $T_2^{R-}S^- * T_1^{R+}$ from A to B is shortened by a path $\tilde{\gamma} = \tilde{\gamma}_1\tilde{\gamma}_2$ of type $T_1^{R+} * T_1^{R+}S^-$ by applying path transformation F_Z to path γ.

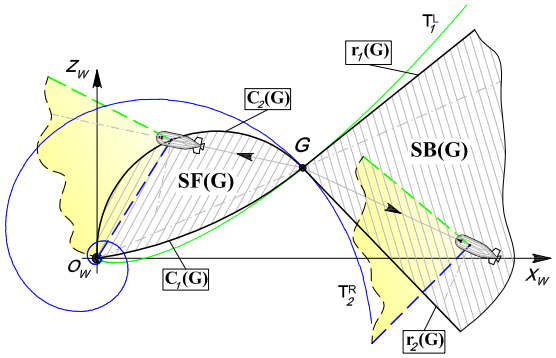

Figure 7: Forward and backward straight path Regions from G for the *Frontal* case, i.e. $0 \leq \Gamma \leq \frac{\delta}{2}$. $SF(G)$ ($SB(G)$) is the set of points reachable from G with a forward (backward) straight line without violating the sensor constraints, see remark 2.

In other words, this theorem states that the shortest path between two points with same distance from the feature evolves completely along points closer to the feature w.r.t. initial and final configurations. The proof of theorem 1 can be found in section A.1 of the Appendix.

An important but straightforward consequence of the theorem is the following

Corollary 1. *For any path in $\mathscr{P}_Q$ with $Q \in C(P)$ there exists a shorter or equal-length path in $\mathscr{P}_Q$ that completely evolves in $D(P)$.*

4 Optimal paths for points on $C(P)$

Our study of the optimal synthesis begins in this section addressing optimal paths from points on $C(P)$. We first need to establish an existence result of optimal paths.

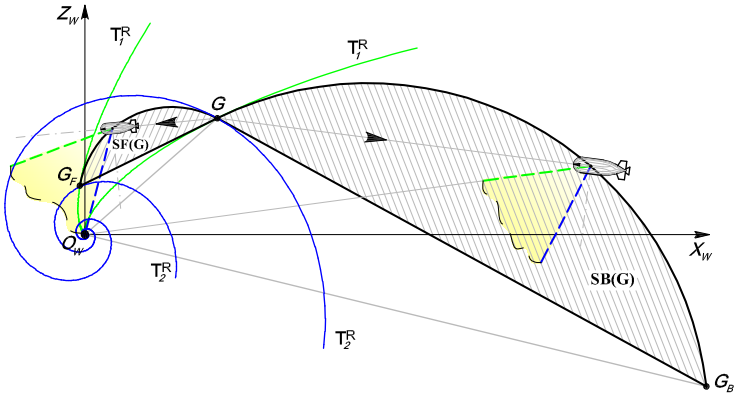

Figure 8: Forward and backward straight path regions from G for the *Side*, *Borderline Side*, and *Lateral* cases, i.e. $\frac{\delta}{2} < \Gamma \leq \frac{\pi-\delta}{2}$. $SF(G)$ ($SB(G)$) is the set of points reachable from G with a forward (backward) straight line without violating the sensor constraints, see remark 3.

Proposition 2. *For any $Q \in C(P)$ there exists a feasible shortest path to P.*

Proof. Because of state constraints (3), and (4), and the restriction of optimal paths in $D(P)$ (corollary 1) the state set is compact. Furthermore, it is possible to give an upper-bound on the optimal path length for all $\Gamma \in [0, \frac{\pi}{2}]$. Indeed, given a point Q at distance ρ from O_w the optimal path to P is shorter or equal to the following paths based on the value of Γ and δ:

- Frontal ($0 \leq \Gamma \leq \frac{\delta}{2}$): $S^+ * S^-$ or $H^+ * H^-$ of length $\rho + \rho_P$;
- Side ($\frac{\delta}{2} < \Gamma < \frac{\pi-\delta}{2}$): $T_{1Q}^{R+} * T_{2P}^{R-}$, of length $\left(\frac{\rho-\rho_N}{\cos\phi_1} + \frac{\rho_P-\rho_N}{\cos\phi_2}\right)$, where N is the intersection point between spirals T_{1Q}^R and T_{2P}^R through Q and P respectively;
- Borderline Side ($\Gamma = \frac{\pi-\delta}{2}$: $T_1^{R+} * C_P^-$) of length $\left(\frac{\rho-\rho_P}{\cos\phi_1} + (\psi_N - \psi_P)\rho_P\right)$, where N is the intersection point between spirals T_1^R and C_P;
- Lateral ($\frac{\pi-\delta}{2} < \Gamma \leq \frac{\pi}{2}$): $T_{2Q}^{L-} * T_{1P}^{R-}$, of length $\left(\frac{\rho-\rho_N}{\cos\phi_2} + \frac{\rho_P-\rho_N}{\cos\phi_1}\right)$, where N is the intersection point between spirals T_{2Q}^L and T_{1P}^R.

The system is also controllable because there always exists an intersection point between two spirals (even if degenerated in half–lines or circles) with different characteristic angle even if both clockwise or counterclockwise around the feature. Hence, Filippov existence theorem for Lagrange problems can be invoked [Cesari, 1983]. □

In the following we provide a set of propositions that completely describe a sufficient optimal finite language $\mathscr{L}_O$ for all values of $\Gamma \in [0, \frac{\pi}{2}]$.

Definition 3. *For any starting point $G = (\rho_G, \psi_G)$, let $SF(G)$ ($SB(G)$) be the set of all points reachable from G with a forward (backward) straight line without violating the sensor constraints.*

Let $C_i(G)$ denote the circular arcs from G to O_w such that, $\forall V \in C_i(G)$ with $\psi_V \in [\psi_G - |\phi_1|, \psi_G]$ (or $\psi_V \in [\psi_G, \psi_G + |\phi_2|]$), $\widehat{GVO_w} = \pi - |\phi_i|$, $i \in \{1, 2\}$.

Remark 2. *Based on simple geometric considerations, for any starting point $G = (\rho_G, \psi_G)$, for $0 \leq \Gamma \leq \frac{\delta}{2}$ (Frontal Case), $SF(G)$ is the region between borders ∂SF_1 and ∂SF_2, where $\partial SF_1(G) = C_1(G)$ and $\partial SF_2(G) = C_2(G)$ (see figure 7). Notice that, $SF(G)$ lays completely in the circle with center in O_w and radius ρ_G. In the particular case in which $\Gamma = \frac{\delta}{2}$ (Borderline Frontal Case), $\partial SF_1(G)$ degenerates in the segment ($\overline{GO_w}$) between G and O_w.*

As a consequence of remark 2, $SF(G)$ is tangent in G to T_1^L (or H) and T_2^R.

Remark 3. *For any starting point $G = (\rho_G, \psi_G)$, and for $\frac{\delta}{2} < \Gamma \leq \frac{\pi}{2}$ (Side and Lateral cases), let $G_F = (\rho_G \frac{\sin\phi_1}{\sin\phi_2}, \psi_G + (\phi_2 - \phi_1)) \in C_2(G)$, i.e. such that $\widehat{O_w G G_F} = \phi_1$ (cf. figures 8 and 9, respectively). Naming with $C_{G_F} \subset C_2(G)$ the arc between G and G_F, $SF(G)$ is the region between arc $\partial SF_2(G) = C_{G_F}$ and segment $\overline{GG_F}$. Notice that, for the Lateral case $SF(G)$ does not lay completely in the circle with center O_w and radius ρ_G. In the particular case in which $\Gamma = \frac{\pi - \delta}{2}$ (Borderline Side Case), $\partial SF_2(G)$ becomes the semicircle from G to $G_F \equiv O_w$ with diameter ρ_G.*

As a consequence of remark 3, $SF(G)$ is tangent in G to T_1^R and T_2^R (or C). Moreover, $SF(G)$ is tangent in G_F to T_1^R and T_2^R (or C), see figure 8.

A generalization of map f_Q (see definition 1) is a map that transforms the whole $\mathbb{R}^2$ rotating and scaling the point Q in a given generic point G not necessarily in P as f_Q does. Let $F : \mathbb{R}^2 \backslash (0,0) \to \mathbb{R}^2$ with $F(Q) = f_Q(G) = \left(\frac{\rho_G^2}{\rho_Q}, 2\psi_G - \psi_Q\right)$. The map F has some properties that make it very useful to the study of our problem in a way which is to some extent similar to what described (for a different F map) in [Salaris et al., 2010]. Indeed, this map is continuous and is an involution, i.e. $F(F(Q)) \equiv Q$, hence $F^{-1} = F$. The invariant set of F is the circle centered in O_w through G. Notice also that, if Q is inside this circle, $F(Q)$ is outside, and vice versa.

Remark 4. *Notice that, F maps points of a forward straight line path from G in points of a backward straight line path from G. As a consequence, borders defined in remarks 2 and 3 are mapped in borders of $SB(G)$ regions of definition 3 as described in the following proposition.*

Proposition 3. *Map F transforms arcs of a circle $C_i(G)$ in half–lines from G and forming an angle $\psi_G - \phi_i$ with the X_w axis.*

Proof. Points of $C_i(G)$ have coordinates $(\rho_G \sin(\phi_i - \psi + \psi_G)/\sin\phi_i, \psi)$ with $\psi \in [\psi_G - |\phi_1|, \psi_G]$ (or $\psi \in [\psi_G, \psi_G + |\phi_2|]$). Such points are mapped in $(\rho_G \sin\phi_i / \sin(\phi_i - \psi + \psi_G), 2\psi_G - \psi)$. On the other hand, the straight line from G forming an angle $\psi_G + \phi_i$ with the X_w axis is described by the equation

$$y = \tan(\psi_G - \phi_i)x - \rho_G \frac{\sin\phi_i}{\cos(\psi_G - \phi_i)}.$$

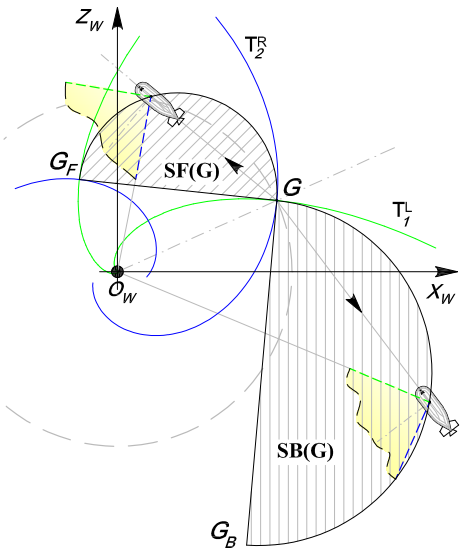

Figure 9: Forward and backward straight path Regions from G for $\frac{\pi-\delta}{2} \leq \Gamma \leq \frac{\pi}{2}$. $SF(G)$ ($SB(G)$) is the set of points reachable from G with a forward (backward) straight line without violating the sensor constraints, see remark 3.

Rewriting this equation in polar coordinates, it is straightforward to check that it is satisfied by the image of $C_i(G)$ under F, hence the thesis. □

Remark 5. *For $0 \leq \Gamma \leq \frac{\delta}{2}$ (Frontal Case), let $r_i(G)$ denote the half–lines from G forming an angle $\psi_G - \phi_i$ with the X_w axis (cf. figure 7). $SB(G)$ is the cone delimited by $\partial SB_1(G) = r_1(G)$ and $\partial SB_2(G) = r_2(G)$, outside circle with center in O_w and radius ρ_G. Moreover, for $\frac{\delta}{2} < \Gamma \leq \frac{\pi}{2}$ (Side and Lateral cases), consider the rotation and scale that map G_F in G and G in $G_B = F(G)$ we have $SB(G) \equiv SF(G_B)$, hence $\partial SB_1(G) = \partial SF_1(G_B)$ and $\partial SB_2(G) = \partial SF_2(G_B)$. Moreover, for all points V on the circular arc C_{G_B} from G_B to G, angle $\widehat{G_BVO_w} = \pi - |\phi_2|$, and angle $\widehat{O_wG_BG} = \phi_1$.*

This remark is a straightforward consequence of proposition 3.

Proposition 4. *If an optimal path from Q to P includes a segment of type S^+ (S^-) with extremes in G, K, then either $K = P \in SF(G)$ ($K = P \in SB(G)$) or $K \in \partial SF_1(G) \cup \partial SF_2(G)$ ($K \in \partial SB_1(G) \cup \partial SB_2(G)$).*

Proof. Consider the case of a segment of type S^+, if $K \notin SF(G)$ the straight line violates either one of sensor constraints. Furthermore, if $K \in SF(G)$ but $K \notin \partial SF_1(G) \cup \partial SF_2(G)$ and $P \notin SF(G)$ the sub-path from K to P intersects $\partial SF_1(G) \cup \partial SF_2(G)$ in K'. Hence, γ could be shortened by replacing the sub–path from G to K' through K with the segment $\overline{GK'}$. If $P \in SF(G)$, then by the optimality principle $K = P$. For a segment of type S^- a similar proof can be followed. □

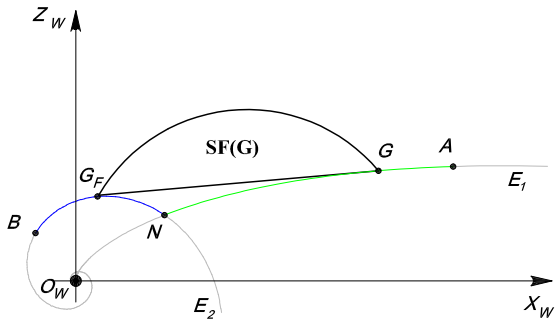

Figure 10: Construction of a path shorter than $E_1^+ * E_2^+$ for $\frac{\delta}{2} < \Gamma \leq \frac{\pi-\delta}{2}$ (cf. theorem 3).

4.1 The Sufficient Family of Optimal Paths

Based on all the above properties, we are now able to obtain a sufficient family of optimal paths by excluding particular sequences of extremals. Notice that results obtained in this section are not a direct consequence of theorems provided in [Salaris et al., 2010]. Indeed, the asymmetry of the FOV with respect to the direction of motion leads to a more complex analysis of paths that may be excluded from the finite sufficient optimal family. For example, in the Side case paths along which the vehicle points toward the feature are no more feasible. Furthermore, with respect to [Salaris et al., 2010], new extremal sequences must be evaluated and possibly excluded from the finite family.

Theorem 2. *Any path consisting in a sequence of a backward extremal arc followed by a forward extremal arc is not optimal.*

The proof of this theorem, whose details can be found in section A.2 of the Appendix, is based on the fact that for continuity of paths, for any sequence of a backward extremal followed by a forward one, there exist points A and B along the path that verify hypothesis of Theorem 1.

Theorem 3. *Any path consisting in a sequence of extremal arcs E_i and E_j followed in the same direction is not optimal for any $i, j \in \{1,2\}$ with $i \neq j$.*

Proof of this theorem can be found in section A.3 of the Appendix and it is based on the fact that for any values of Γ and δ and for any path γ consisting in a sequence of extremal arcs E_i and E_j followed in the same direction ($i, j \in \{1,2\}$ with $i \neq j$) there exists a sub–path of γ that can be shortened by a straight line. For example, referring to figure 10, in the Side case ($\frac{\delta}{2} < \Gamma < \frac{\pi-\delta}{2}$), there always exists a point G along E_1 between A and N such that $SF(G)$ intersects E_2 between N and B. Hence, γ can be shortened by $\overline{GG_F}$.

Notice that the feasible sequences consisting of two extremals that we still need to be discussed, and eventually excluded, are those starting or ending with S followed in any direction ($E_i^+ E_i^-$ and $E_i^- E_i^+$, with $i \in \{1,2\}$, are obviously not optimal).

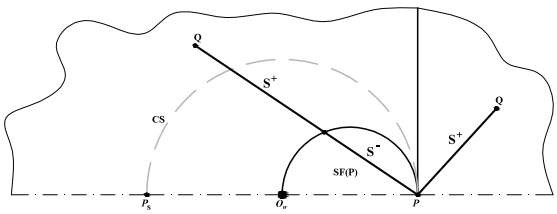

Figure 11: Shortest paths in the Symmetric Frontal case with $\delta = \pi$.

Proposition 5. *From any starting point A, any path γ of type $S^+ * E_2^+$ ($S^- * E_1^-$) and $S^+ * E_1^-$ to B can be shortened by a path of type $S^+E_2^+$ ($S^-E_1^-$), S^+ (S^-) or $E_2^+ * E_1^-$.*

Proposition 6. *For $\frac{\delta}{2} \leq \Gamma \leq \frac{\pi}{2}$ (Side and Lateral cases), from any starting point A, any path γ of type $S^+ * E_1^+$ ($S^- * E_2^-$) or $S^+ * E_2^-$ can be shortened by a path of type S^+ (S^-), $E_1^+S^+$ ($E_2^-S^-$) or $E_1^+ * E_2^-$.*

Proposition 7. *For $0 \leq \Gamma < \frac{\delta}{2}$ (Frontal case), from any starting point A, any path γ of type $S^+ * E_1^+$ or $S^+ * E_2^-$ can be shortened by a path of type S^+, $S^+E_1^+$ or $E_1^+ * E_2^-$. Furthermore, for any path γ of type $S^- * E_2^-$ or $S^- * E_1^-$ can be shortened by a path of type S^-, $E_2^-S^-$ or $E_1^+ * E_2^-$.*

Proposition 8. *For $0 \leq \Gamma < \frac{\delta}{2}$ (Frontal case), from any starting point A, any path γ of type $S^+ * S^-$ can be shortened if the angle between arc S^+ and arc S^- is less than $\psi_V \triangleq \phi_1 + \phi_2 + \frac{\sin(\phi_1+\phi_2)}{\cos\phi_1\cos\phi_2}\left[2\ln\left(\frac{\sin(\phi_1+\phi_2)}{\cos\phi_1+\cos\phi_2}\right) + \ln\sin\phi_1 + \ln\sin\phi_2\right]$.*

Proofs of previous propositions are reported in Appendix, section A.4.

Remark 6. *Notice that, based on proposition 8, when $\delta > \psi_V$ the switching point between S^+ and S^- is not necessarily O_w. For example, if $\delta = \pi$ from any point Q on the motion plane to P the optimal path is of type $S^+ * S^-$ as shown in figure 11 and the switching point is on the border of $SF(P)$.*

Remark 7. *Notice that if a sequence of extremals from A to B is not optimal, also the path from B to A following extremals in reverse order and opposite direction is not optimal. For example, $E_1^+ * S^-$ is not optimal since it is the inverse path of type $S^+ * E_1^-$ that is not optimal for proposition 5.*

Proposition 9. *For $\frac{\delta}{2} \leq \Gamma \leq \frac{\pi}{2}$ (Side and Lateral cases), $S^+ * S^-$ path can be shortened by paths of type $E_2^+ * S^-$, $S^+ * E_2^+$, $E_1^+ * S^+$ and $E_1^+S^+$.*

The proof of this proposition is reported in Appendix, section A.4.

By using all previous results, a sufficient family of optimal paths is obtained in the following important theorem.

Theorem 4. *For $0 \leq \Gamma \leq \frac{\delta}{2}$, i.e. Frontal case, and for any $Q \in D(P)$ to P there exists a shortest path of type $S^+E_1^+ * E_2^-S^-$ or of type $S^+E_2^+ * E_1^-S^-$. For $\frac{\delta}{2} < \Gamma \leq \frac{\pi}{2}$, i.e. Side and Lateral cases, and for any $Q \in D(P)$ to P there exists a shortest path of type $E_1^+ * E_2^-S^-E_1^-$ or of type $E_1^+S^+E_2^+ * E_1^-$.*

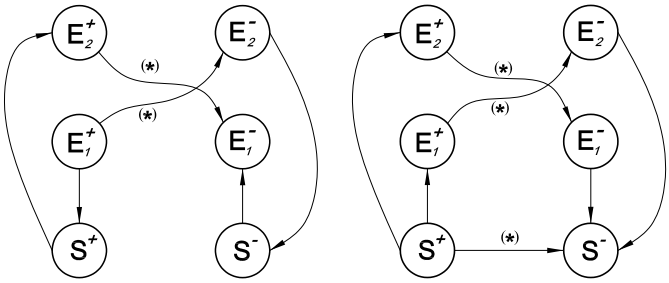

(a) Side and Lateral cases ($\frac{\delta}{2} < \Gamma \leq \frac{\pi}{2}$).

(b) Frontal case ($0 \leq \Gamma \leq \frac{\delta}{2}$).

Figure 12: Representation of finite optimal language $\mathscr{L}_O$ from points in $D(P)$ based on extremals (nodes) and feasible concatenations (edges). Symbol $(*)$ on the edge represents a non–smooth concatenation.

Proof. According to all propositions above several concatenations of extremal have been proved to be non optimal. Considering extremals as node and, possibly optimal, concatenations of extremal as edges of a graph, the sufficient optimal languages $\mathscr{L}_O$ from Q in $D(P)$, for different values of Γ and δ, are described in figure 12. Indeed, it is straightforward to observe that the number of switches between extremals is finite and less or equal to 3, for any value of Γ and δ. Hence, the thesis. □

Remark 8. *Notice that, previous theorem describes a sufficient family of optimal paths, i.e. path of type $S^+E_1^+ * E_2^-S^-$ or of type $S^+E_2^+ * E_1^-S^-$ for the Frontal case and path of type $E_1^+ * E_2^-S^-E_1^-$ or of type $E_1^+S^+E_2^+ * E_1^-$ for the Side and Lateral cases. Of course, in those family are included also all its degenerate cases, i.e. paths obtained from previous ones with one or more zero length arcs.*

We now study the length of extremal paths from $C(P)$ to P in the sufficient family above. Based on properties of map F_Q, it is sufficient to study the length of paths only from points $Q = (\rho_P, \psi_Q)$ on the semicircle of $C(P)$ in the upper-half plane (denoted by *CS*). Indeed, up to a clockwise rotation of ψ_Q, optimal paths from $Q' = (\rho_P, -\psi_Q)$ in the lower-half plane is easily obtained, and hence also the loci of switching points between extremal arcs.

In order to simplify the analysis, we will consider separately three cases: Frontal Case, Side Case, and Lateral Case. Moreover, optimal synthesis of *CS* will be determined for each case in following sections. The optimal synthesis on the whole $C(P)$ can be obtained applying map F_Q to path starting from points on *CS*.

4.2 Frontal Case

Based on theorem 4, let us consider a path of type $S^+T_1^{L+} * T_2^{R-}S^-$ from points $Q = (\rho_P, \psi_Q)$ on *CS*. Referring to figure 13, let the switching points along optimal path be denoted by N, M_1 and M_2. Moreover, in order to do the analysis, it is useful to

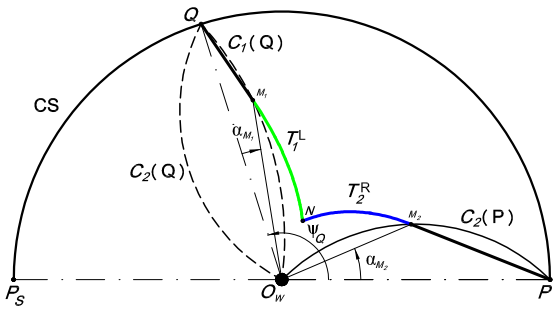

Figure 13: Path of type $S^+T_1^{L+} * T_2^{R-}S^-$ or the degenerate case of type $T_1^{L+} * T_2^{R-}$, $S^+ * S^-$, and $T_1^{L+} * T_2^{R-}S^-$ from $Q \in CS$.

parameterize the family by the angular value α_{M_1} of the switching point M_1 along the arc $C_1(Q)$ between Q and O_w and the angular value α_{M_2} of the switching point M_2 along the arc $C_2(P)$ between P and O_w.

Theorem 5. *For any point $Q \in CS$, length L of a path $\gamma \in \mathscr{P}_Q$ of type $S^+T_1^{L+} * T_2^{R-}S^-$ is:*

$$\begin{aligned} L &= \rho_P \left(\frac{\cos\alpha_{M_1}}{\cos\phi_1} + \frac{\cos\alpha_{M_2}}{\cos\phi_2} \right) + \\ &- \rho_P \frac{\cos\phi_1 + \cos\phi_2}{\cos\phi_1 \cos\phi_2} \left[\rho_P \frac{\sin(\phi_1 - \alpha_{M_1})}{\sin\phi_1} \right]^{\frac{t_2}{t_1+t_2}} \cdot \\ &\cdot \left[\rho_P \frac{\sin(\phi_2 - \alpha_{M_2})}{\sin\phi_2} \right]^{\frac{t_1}{t_1+t_2}} e^{\left(\alpha_{M_1} + \alpha_{M_2} - \psi_Q\right) \frac{t_1 t_2}{t_1+t_2}}, \end{aligned} \tag{11}$$

where both ϕ_1 and ϕ_2 assume values in $]0, \frac{\pi}{2}[$, and with $t_1 = 1/\tan\phi_1$ and $t_2 = 1/\tan\phi_2$. In the extreme cases $\phi_1 = \phi_2 = 0$ and $|\phi_1| = |\phi_2| = \frac{\pi}{2}$, we have $L = 2\rho_P$ and $L = 2\rho_P \sin\frac{\psi_Q}{2}$, respectively.

The analytical expression for the length L is based on a direct computation, using similar arguments to those used to prove Theorem 3 in [Salaris et al., 2010].

Having an analytical expression for the length of the path as a function of three parameters α_{M_1}, α_{M_2} and ψ_Q, we can minimize the length within the sufficient family. Notice that we need only to consider $\alpha_{M_2} \in [0, \phi_2]$, and $\alpha_{M_1} \in [0, -\phi_1]$ for the geometrical considerations above on $C_2(Q)$ (see remark 2).

Theorem 6. *Given $Q = (\rho_P, \psi_Q) \in CS$, and both ϕ_1 and ϕ_2 belong to $]0, \pi/2[$, referring to figure 14,*

- *for $0 < \psi_Q \leq \psi_M \triangleq -\frac{\sin(\phi_1+\phi_2)}{\cos\phi_1\cos\phi_2} \ln\left(\frac{\sin\phi_2 \sin(\phi_1+\phi_2)}{\cos\phi_1+\cos\phi_2}\right)$, the optimal path is of type $T_1^{L+} * T_{2P}^{R-}$;*

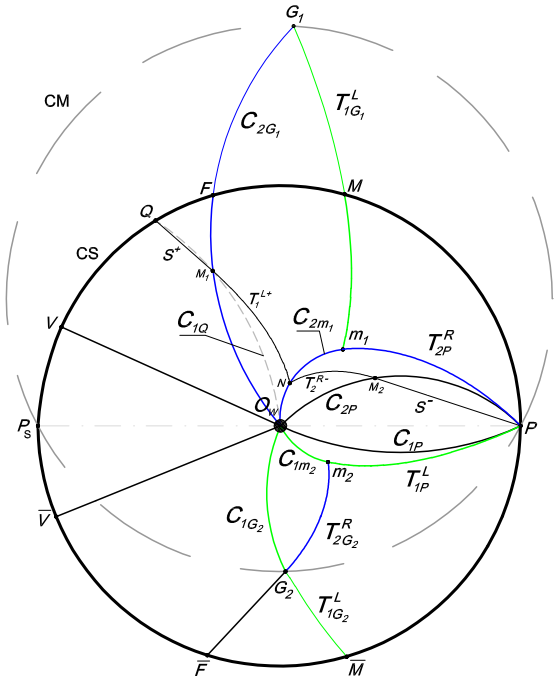

Figure 14: Frontal ($0 < \Gamma < \frac{\delta}{2}$): optimal path from $Q \in CS$ between F and V. The locus of switching points between extremals S^+ and T_1^{L+} is arc $C_2(G_1) \equiv C_{2G_1}$, whereas between extremals T_1^{L+} and T_2^{R-} is arc $C_2(m_1) \equiv C_{2m_1}$.

- *for* $\psi_M < \psi_Q \leq \psi_F \triangleq \phi_2 - \phi_1 + \psi_M - \frac{\sin(\phi_1+\phi_2)}{\cos\phi_1\cos\phi_2} \ln\left(\frac{\sin\phi_1 \sin(\phi_1+\phi_2)}{\cos\phi_1+\cos\phi_2}\right)$, *the optimal path is of type* $T_1^{L+} * T_2^{R-} S^-$;

- *for* $\psi_F < \psi_Q < \psi_V \triangleq 2\phi_1 + \psi_F$, *the optimal path is of type* $S^+ T_1^{L+} * T_2^{R-} S^-$;

- *for* $\psi_V \leq \psi_Q < \pi$, *the optimal path is of type* $S^+ * S^-$

Previous results have been obtained computing first and second derivatives of length L and by using nonlinear minimization techniques.

We are now interested in determining the locus of switching points between extremals in optimal paths from CS. Based on a similar procedure followed in [Salaris et al., 2010], the loci of switching points are (see figure 14):

- For $Q \in C(P)$ with $0 \leq \psi_Q \leq \psi_M$, i.e. between P and M, the switching locus is the arc of T^R_{2P} within the extreme points P and $m_1 = \left(\rho_P \frac{\sin(\phi_1+\phi_2)\sin\phi_2}{\cos\phi_1+\cos\phi_2}, \frac{1}{t_2}\ln\left(\frac{\cos\phi_1+\cos\phi_2}{\sin(\phi_1+\phi_2)\sin\phi_2}\right)\right)$ (included).

- For $Q \in C(P)$ with $\psi_M < \psi_Q \leq \psi_F$, i.e. between M and F, the loci of switching points M_2, N are the arcs $C_2(P)$, $C_2(m_1)$, respectively.
- For $Q \in C(P)$ with $\psi_F < \psi_Q < \psi_V$, i.e. between F and V, the loci of switching points M_1, N, and M_2 are the arcs $C_2(G_1)$, $C_2(m_1)$, and $C_2(P)$ with $G_1 = (\rho_P \frac{\sin\phi_2}{\sin\phi_1}, \psi_V - \phi_1 - \phi_2)$ outside CS, respectively.
- Finally, for $Q \in C(P)$ with $\psi_V \leq \psi_Q \leq \pi$ the loci of switching points is point O_w.

Remark 9. *Notice that, when $\phi_2 = -\phi_1 = \phi$, $\Gamma = 0$ and the synthesis proposed in [Salaris et al., 2010] is obtained.*

Remark 10. *Points P, G_1 and $G_2 = f_{G_2}(P) = (\rho_P \frac{\sin\phi_1}{\sin\phi_2}, -\psi_{G_1})$ belong to a circle denoted by CM in figure 14, passing through P_s. This circle is centered in a point whose cartesian coordinates are $(0, \alpha)$ where*

$$\alpha = \rho_P \frac{\sin^2\phi_1 - \sin^2\phi_2}{2\sin\xi \sin\phi_1 \sin\phi_2},$$

and radius

$$R = \frac{\rho_P}{2\sin\xi}\sqrt{\frac{\sin^2\phi_1}{\sin^2\phi_2} + \frac{\sin^2\phi_2}{\sin^2\phi_1} - 2\cos(2\xi)},$$

where

$$\xi = \frac{t_1 + t_2}{t_1 t_2}\ln\left(\frac{\cos\phi_1 + \cos\phi_2}{\sin(|\phi_1| + \phi_2)}\right) + \frac{1}{t_1}\ln(\sin|\phi_1|) - \frac{1}{t_2}\ln(\sin\phi_2).$$

Moreover, if $\phi_2 = -\phi_1 = \phi$ circle CM becomes circle $C(P)$.

4.2.1 Borderline Frontal Case (see figure 15)

In this case, $\Gamma = \frac{\delta}{2}$ and angle $\phi_1 = 0$. Hence, spiral T_1^L becomes a straight line through O_w, denoted by H. The subdivision of CS can be obtained replacing $\phi_1 = 0$ in theorem 6. Notice that, $F \equiv V$ and $\psi_V = \phi_2 + \psi_M$ where $\psi_M = -\tan\phi_2 \ln\left(\frac{\sin^2\phi_2}{1+\cos\phi_2}\right)$. Moreover, $m_1 = \left(\rho_P \frac{\sin^2\phi_2}{1+\cos\phi_2}, -\tan\phi_2 \ln\left(\frac{\sin^2\phi_2}{1+\cos\phi_2}\right)\right)$, $G_1 \to \infty$, $G_2 \equiv m_2 \equiv O_w$. As a consequence, for $0 \leq \psi_Q \leq \psi_M$ the optimal path is $H^+ * T_{2P}^{R-}$ and the locus of switching point is the arc of spiral T_{2P}^R between P and m_1 (included); for $\psi_M \leq \psi_Q < \psi_V \equiv \psi_F$, the optimal path is $H^+ * T_2^{R-} S^-$ and the loci of switching points between extremals H^+ and T_2^{R-} and between T_2^{R-} and S^- are $C_2(m_1)$ and $C_2(P)$, respectively. Finally, for $\psi_V \leq \psi_Q \leq \pi$ the optimal path is $S^+ * S^-$, hence, the locus of switching points is O_w.

Notice that, in this case, circle CM degenerates on X_w, i.e. a circle with infinity radius, as shown in figure 15.

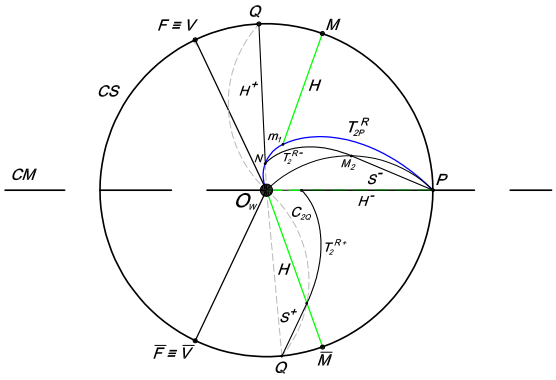

Figure 15: Borderline Frontal ($\Gamma = \frac{\delta}{2}$): optimal path from $Q \in C(P)$ between M and V ($\overline{M}$ and $\overline{V}$). On CS, the optimal path is $H^+T_2^{R-} * S^-$, and the locus of switching points between extremals H^+ and T_2^{R-} is arc $C_2(m_1)$, whereas between extremals T_2^{R-} and S^- is arc $C_2(P)$. On the lower-half plane, for $Q \in C(P)$ between $\overline{M}$ and $\overline{V}$, the optimal path is $S^+T_2^{R+} * H^-$ and the locus of switching points between extremals S^+ and T_2^{R+} is spiral arc H, whereas between extremals T_2^{R+} and S^- is the segment $\overline{PO}_w$.

4.3 Side Case

Let us consider the length of extremal paths of type $T_1^{R+} * T_2^{R-}S^-T_1^{R-}$ from points $Q = (\rho_P, \psi_Q)$ on the semicircle of $C(P)$ in the upper-half plane, i.e. CS. Referring to figure 16, let the switching points of the optimal path be denoted by N, M_1 and M_2 or $\overline{N}$, $\overline{M}_1$ and $\overline{M}_2 \equiv P$, respectively, depending on the angular values α_{M_1} or $\alpha_{\overline{M}_1}$. Moreover, in order to do the analysis, it is useful to parameterize the family by the angular value $\alpha_{\overline{M}_1}$ of the switching point $\overline{M}_1$ along the arc $C_2(P)$ between P and P_F or the angular value α_{M_1} of the switching point M_1 along the extremal E_1 between P_F and O_w.

Theorem 7. *For any point $Q \in CS$, length L of a path $\gamma \in \mathscr{P}_Q$ (see figure 16) of type $T_1^{R+} * T_2^{R-}S^-T_1^{R-}$ is:*

- *for $0 \leq \alpha_{\overline{M}_1} \leq \phi_2 - \phi_1$, i.e. from P to P_F (notice that the last arc has zero length):*

$$L = \rho_P \left\{ \frac{\cos\alpha_{\overline{M}_1}}{\cos\phi_2} + \frac{1}{\cos\phi_1} + \right.$$
$$\left. - \frac{\cos\phi_1 + \cos\phi_2}{\cos\phi_1\cos\phi_2} e^{\left(\psi_Q - \alpha_{\overline{M}_1}\right)\frac{t_1 t_2}{t_2 - t_1}} \left(\frac{\sin\left(\phi_2 - \alpha_{\overline{M}_1}\right)}{\sin\phi_2} \right)^{-\frac{t_1}{t_2 - t_1}} \right\}, \tag{12}$$

- *for $\alpha_{M_1} \geq \phi_2 - \phi_1$, i.e. from P_F to O_w:*

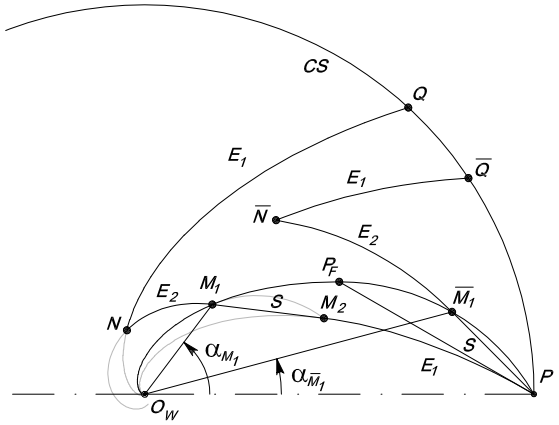

Figure 16: Path of type $E_1^+ * E_2^- S^- E_1^-$ or the degenerate case of type $E_1^+ * E_2^- S^-$ from $Q \in CS$.

$$L = \rho_P \left\{ \frac{2}{\cos\phi_1} + e^{-\alpha_{M_1} t_1} \left[\frac{\cos(\phi_2 - \phi_1)}{\cos\phi_2} - \frac{1}{\cos\phi_1} + \right.\right.$$
$$\left.\left. - \frac{\cos\phi_1 + \cos\phi_2}{\cos\phi_1 \cos\phi_2} e^{[\psi_Q - (\phi_2 - \phi_1)] \frac{t_1 t_2}{t_2 - t_1}} \left(\frac{\sin\phi_1}{\sin\phi_2} \right)^{-\frac{t_1}{t_2 - t_1}} \right] \right\}, \tag{13}$$

with $t_1 = 1/\tan\phi_1$ *and* $t_2 = 1/\tan\phi_2$.

The proof of this theorem is reported in Appendix, section A.5. Having an analytical expression for length L of the path as a function of two parameters α_{M_1} or $\alpha_{\overline{M}_1}$ and ψ_Q, we are now in a position to minimize the length within the sufficient family.

Theorem 8. *Given a point $Q \in CS$ (see figure 17),*

- *for $0 \leq \psi_Q \leq \psi_{R_1} := \frac{\sin(\phi_2 - \phi_1)}{\cos\phi_1 \cos\phi_2} \ln\left(\frac{\cos\phi_1 + \cos\phi_2}{\sin\phi_2 \sin(\phi_2 - \phi_1)} \right)$, i.e. between P and R_1, optimal path is of type $T_1^{R+} * T_2^{R-}$;*
- *for $\psi_{R_1} \leq \psi_Q \leq \psi_{R_2}$ with $\psi_{R_2} := (\phi_2 - \phi_1) + \psi_{R_1} + \tan\phi_2 \ln\left(\frac{\sin\phi_1}{\sin\phi_2} \right)$, i.e. between R_1 and R_2, optimal path is of type $T_1^{R+} * T_2^{R-} S^-$;*
- *for $\psi_{R_2} \leq \psi_Q \leq \pi$, the optimal path is $T_1^{R+} * T_1^{R-}$ through O_w.*

Moreover, for $\psi_Q = \psi_{R_2}$, any optimal path of type $T_1^{R+} * T_2^{R-} S^- T_1^{R-}$ turns out to have the same length of optimal path $T_1^{R+} * T_1^{R-}$. Hence, for $\psi_Q = \psi_{R_2}$ also $T_1^{R+} * T_2^{R-} S^- T_1^{R-}$ is optimal.

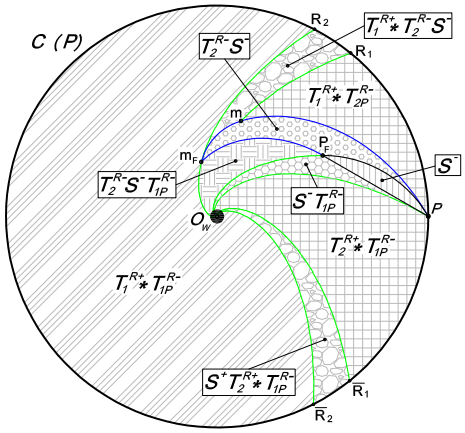

Figure 17: Side case ($\frac{\delta}{2} < \Gamma < \frac{\pi-\delta}{2}$): optimal synthesis on $C(P)$ and within $D(P)$. From points Q on spiral arc T_1^R between R_2 and m_F, paths of type $T_1^{R+} * T_2^{R-} S^-$ and $T_1^{R+} * T_2^{R-} S^- T_{1P}^{R-}$ have the same length and hence both optimal paths.

Previous results have been obtained computing first and second derivatives of L and by using nonlinear minimization techniques.

We are now interested in determining the locus of switching points between extremals in optimal paths.

Proposition 10. *For $Q \in CS$ with $0 \leq \psi_Q \leq \psi_{R_1}$, the switching locus is the arc of $E_2 \equiv T_{2P}^{R-}$ between P and $m = (\rho_P \frac{\sin\phi_2 \sin(\phi_2-\phi_1)}{\cos\phi_1+\cos\phi_2}, \psi_M)$ (included), where $\psi_m = \tan\phi_2 \ln\left(\frac{\rho_P}{\rho_m}\right)$.*

Proof. From theorem 8, the optimal path from $Q \in CS$ to P is of type $T_1^{R+} * T_2^{R-}$ (see figure 17), with $T_2^{R-} \equiv T_{2P}^{R-}$, hence the switch occurs on T_{2P}^{R-}. For $\psi_Q = \psi_{R_1}$ the intersection between T_1^{R+} and T_2^{R-} is m. □

Proposition 11. *For $Q \in CS$ with $\psi_{R_1} < \psi_Q \leq \psi_{R_2}$, the loci of switching points $\overline{M}_1$ and $\overline{N}$ are the $\partial SF_2(P)$ and $\partial SF_2(m)$.*

Proof. For $Q \in CS$ with $\psi_{R_1} < \psi_Q < \psi_{R_2}$, from theorem 8 we have $\overline{M}_1 \in \partial SF_2(P)$ (see figure 17). Furthermore, substituting the optimal values of α_{M_1}, obtained computing first and second derivatives of L, coordinates in equations (20) and (21) of the intersection point $\overline{N}$ between $E_1 \equiv T_1^{R+}$ through Q and $E_2 \equiv T_2^{R-}$ through $\overline{M}_1$ we obtain $\overline{N} \in \partial SF_2(m)$ (see section A.5 in the Appendix). □

Finally, for $Q \in CS$ with $\psi_{R_2} \leq \psi < \pi$, the switching locus reduces to the origin O_w since two extremal E_i intersect only in the origin for $i = 1, 2$.

4.3.1 Borderline Side Case

In this case $\Gamma = \frac{\pi-\delta}{2}$ and angle $\phi_2 = \frac{\pi}{2}$. Hence, spiral T_2^R degenerates in a circle centered in O_w, denoted by C. The subdivision of CS can not be obtained directly from

the Side case replacing $\phi_2 = \frac{\pi}{2}$ in all previous results although, as shown in figure 18, the subdivision of $C(P)$ is quite similar. Indeed, let us consider the length of extremal paths of type $T_1^{R+} * C^- S^- T_1^{R-}$ from point $Q \in CS$. Moreover, in order to do the analysis, let the switching points of extremal path be denoted by N, M_1 and M_2 or $\overline{N}$, $\overline{M}_1$ and $\overline{M}_2 \equiv P$, respectively, depending on the angular values α_{M_1} or $\alpha_{\overline{M}_1}$, similarly to figure 16 with $E_2 = C$.

Theorem 9. *For any point $Q \in CS$, length L of a path $\gamma \in \mathscr{P}_Q$ of type $T_1^{R+} * C^- S^- T_1^{R-}$ is:*

- *for $0 \leq \alpha_{\overline{M}_1} \leq \frac{\pi}{2} - \phi_1$, i.e. from P to P_F (notice that the last arc has zero length):*

$$L = \rho_P \Big\{ \sin \alpha_{\overline{M}_1} + \frac{1 - \cos \alpha_{\overline{M}_1}}{\cos \phi_1} + \cos \alpha_{\overline{M}_1} \left(\psi_Q - \tan \phi_2 \ln(\cos \alpha_{\overline{M}_1}) - \alpha_{\overline{M}_1} \right), \tag{14}$$

- *for $\alpha_{M_1} \geq \frac{\pi}{2} - \phi_1$, i.e. from P_F to O_w:*

$$L = \rho_P \left\{ \frac{2}{\cos \phi_1} + \sin \phi_1 \; e^{(\alpha_{M_1} - \frac{\pi}{2} + \phi_1) t_1} \frac{1 + \sin \phi_1}{\cos \phi_1} + + \psi_Q - \phi_1 - \frac{\pi}{2} + \tan \phi_1 \ln(\sin \phi_1) \right\}, \tag{15}$$

with $t_1 = 1/\tan \phi_1$.

The length L can be computed using techniques similar to those used for theorem 7. Having an analytical expression for the length of the path as a function of two parameters α_{M_1} or $\alpha_{\overline{M}_1}$ and ψ_Q, we are now in a position to minimize the length.

Theorem 10. *Given a point $Q \in CS$ (see figure 18),*

- *for $0 \leq \psi_Q \leq \psi_{R_1} := \frac{1+\sin \phi_1}{\cos \phi_1}$, i.e. between P and R_1, optimal path is of type C^- until P;*
- *for $\psi_{R_1} \leq \psi_Q \leq \psi_{R_2}$ with $\psi_{R_2} := (\frac{\pi}{2} - \phi_1) + \psi_{R_1} + \tan \phi_1 \ln(\sin \phi_1)$, i.e. between R_1 and R_2, optimal path is of type $T_1^{R+} * C^- S^-$;*
- *for $\psi_{R_2} \leq \psi_Q \leq \pi$ the optimal path is $T_1^{R+} * T_1^{R-}$ through O_w.*

Moreover, for $\psi_Q = \psi_{R_2}$, any optimal path of type $T_1^{R+} * C^- S^- T_1^{R-}$ turns out to have the same length of optimal path $T_1^{R+} * T_1^{R-}$. Hence, for $\psi_Q = \psi_{R_2}$ also $T_1^{R+} * C^- S^- T_1^{R-}$ is optimal.

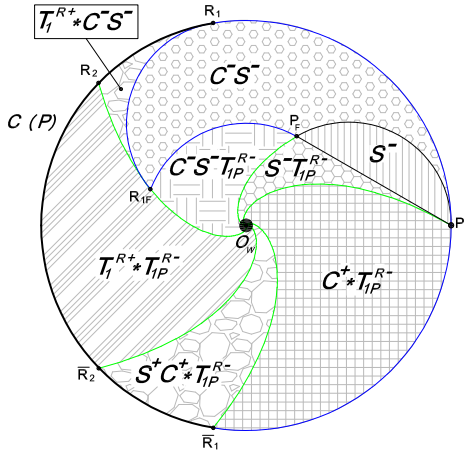

Figure 18: Borderline Side case ($\Gamma = \frac{\pi-\delta}{2}$): optimal synthesis on $C(P)$ and within $D(P)$. From points Q on spiral arc T_1^R between R_2 and $m_{R_{1F}}$, paths of type $T_1^{R+} * C^- S^-$ and $T_1^{R+} * C^- S^- T_{1P}^{R-}$ have the same length and hence both optimal paths.

Previous results have been obtained computing first and second derivatives of L and by using nonlinear minimization techniques.

We are now interested in determining the locus of switching points between extremals in optimal paths. By using a similar argumentation followed in propositions 10 and 11, we have

- for $0 \leq \psi_Q \leq \psi_{R_1}$, the locus of switching point is arc of circle CS between R_1 and P;
- for $\psi_{R_1} < \psi_Q \leq \psi_{R_2}$, the loci of switching points between extremals T_1^{R+} and C^- is arc $\partial F_2(R_1)$, whereas between extremals C^- and S^- is arc $\partial F_2(P)$.

Finally, for $\psi_{R_2} \leq \psi_Q \leq \pi$, the locus of switching points is O_w (see figure 18).

4.4 Lateral and Symmetric Lateral Cases

In this case, $\frac{\pi-\delta}{2} < \Gamma \leq \frac{\pi}{2}$. Spirals have characteristic angles $\phi_1 = \frac{\pi-\delta}{2}$ and $\phi_2 = \frac{\pi+\delta}{2}$, and equations are

$$\rho_1 = \rho_{1o}\, e^{\psi t_1}$$
$$\rho_2 = \rho_{2o}\, e^{\psi t_2},$$

where $t_1 = 1/\tan\left(\frac{\pi-\delta}{2}\right)$, whereas $t_2 = 1/\tan\left(\frac{\pi+\delta}{2}\right) = -t_1$, i.e. two logarithmic spirals, right and left respectively, with the same characteristic angle $\phi = \frac{\pi-\delta}{2}$. The subdivision of the motion plane can be obtained following the same procedure of the Side and Borderline Side cases. Nevertheless, unlike previous cases and as a consequence of remark 3, for $Q \in CS$ with $0 \leq \psi_Q \leq \psi_{R_o} = 2\phi_2 - \pi$, the optimal path is a straight line until P (i.e. S^-).

5 Shortest paths from any point in the motion plane

The synthesis on $C(P)$ induce a partition in regions of $D(P)$. Indeed, for any $Q \in D(P)$, there exists a point $V \in C(P)$ such that the optimal path γ from V to P goes through Q. The Bellmann's optimality principle ensure the optimality of the sub–path from Q to P. For points outside $C(P)$, function F_Q has been defined in (10) in order to transform paths starting from Q inside $C(P)$ in paths starting from $f_Q(P) = \left(\frac{\rho_P^2}{\rho_Q}, -\psi_Q\right)$ outside $C(P)$.

From other properties of F_Q, such as Proposition 1, we have also that an optimal path is mapped into an optimal path. Hence, the optimal synthesis from points outside $C(P)$ can be easily obtained mapping through map F_Q all borders of regions inside $C(P)$.

Proposition 12. *Given a border* $\mathbf{B}$ *and* $Q \in \mathbf{B}$ *map* F_Q *transforms:*

1. $\mathbf{B} = C(P)$ *into itself;*
2. $\mathbf{B} = \partial SF_2(Q)$ *in* $\partial SB_1(f_Q(P))$
3. $\mathbf{B} = \partial SF_1(Q)$ *in* $\partial SB_2(f_Q(P))$
4. $\mathbf{B} = E_i$ *in arcs of the same type (*$i = 1, 2$*)*

The proof of this proposition is based on the properties of the map F_Q, which consists of rotations and scalings, which transform spiral arcs in spiral arcs, and arcs of circles through the origin in straight lines (and viceversa), cf. remark 1. A detailed proof can be found in [Salaris et al., 2010].

Based on Proposition 12, the optimal synthesis of the entire motion plane is reported in figure 19 and figure 20 for the Frontal and Borderline Frontal cases. In figure 21 and figure 22 are reported the optimal synthesis for the Side and the Borderline Side cases. Finally, figure 23 and figure 24 shown the partition of the motion plane for the Lateral and Symmetric Lateral cases.

The subdivision of the motion plane in case of $\frac{\pi}{2} < \Gamma \leq \pi$ can be easily obtained by using that for $0 \leq \Gamma \leq \frac{\pi}{2}$ considering optimal path followed in reverse order, i.e. forward arc in backward arc and vice versa. Finally, a symmetry w.r.t. X_w axis of each subdivision of the motion plane for each $\Gamma \in [0, \pi]$ allows to obtain the corresponding subdivision for $\Gamma \in [-\pi, 0]$.

Finally, it is useful to point out that borders of all regions are arcs of circle, straight lines or logarithmic spirals. Hence, conditions on ρ_Q and ψ_Q determining the inclusion of a point Q in each region can be obtained in terms of a finite number of elementary inequalities. As a consequence, given any initial robot position Q, an algorithm that returns the Region in which robot lays can be easily obtained.

6 Conclusions and future work

A complete characterization of shortest paths for moving bodies with a preferential direction of motion equipped with a general, limited FOV sensor system has been

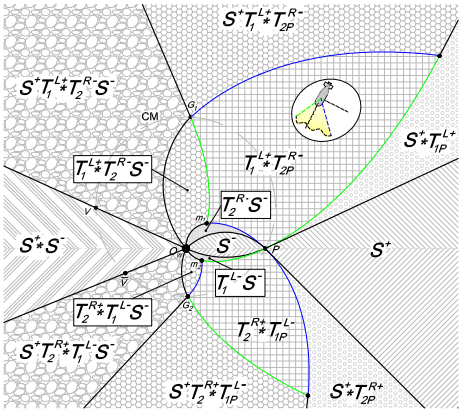

Figure 19: Partition of the motion plane for $0 \leq \Gamma < \frac{\delta}{2}$, i.e. Frontal case.

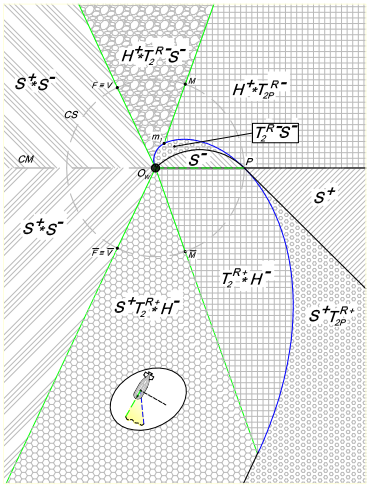

Figure 20: Partition of the motion plane for $\Gamma = \delta/2$, i.e. Borderline Frontal (the right border is aligned with the robot motion direction).

proposed. A finite sufficient family of optimal paths has been determined based on geometrical properties of the considered problem. Finally, a complete shortest path synthesis to reach a point keeping a given feature in sight has been provided. While the problem of keeping in sight, during motion, at least one feature can be considered solved by these results, to obtain the current robot position, at least three features are needed. As a consequence, a generalization of the optimal synthesis would be necessary, providing the shortest paths to a goal keeping in sight more (at least three) features. This is an open problem for future works.

A possible extension of this work is to consider a more realistic sensor, as a camera, with both horizontal and vertical FOV limits pointing to any direction with respect to

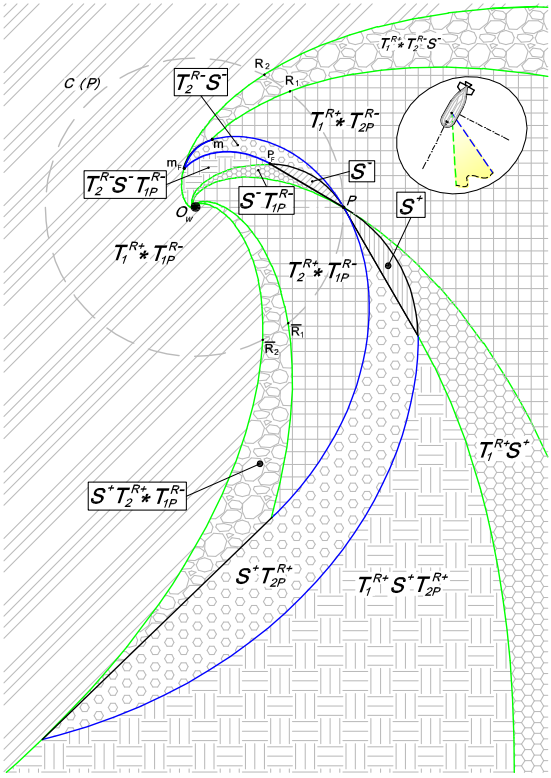

Figure 21: Partition of the motion plane for $\frac{\delta}{2} < \Gamma < \frac{\pi-\delta}{2}$, i.e. Side case.

the direction of motion. Another possible extension would be considering a different minimization problem such as minimum time.

References

Arechavaleta, G., Laumond, J.-P., Hicheur, H., and Berthoz, A. (2008a). On the non-holonomic nature of human locomotion. *Autonomous Robots*, 25:25–35.

Arechavaleta, G., Laumond, J.-P., Hicheur, H., and Berthoz, A. (2008b). An optimality principle governing human walking. *Robotics, IEEE Transactions on*, 24(1):5 –14.

Balkcom, D. and Mason, M. (2006). Time-optimal trajectories for an omnidirectional vehicle. *The International Journal of Robotics Research*, 25(10):985–999.

Bhattacharya, S., Murrieta-Cid, R., and Hutchinson, S. (2007). Optimal paths for landmark–based navigation by differential–drive vehicles with field–of–view constraints. *IEEE Transactions on Robotics*, 23(1):47–59.

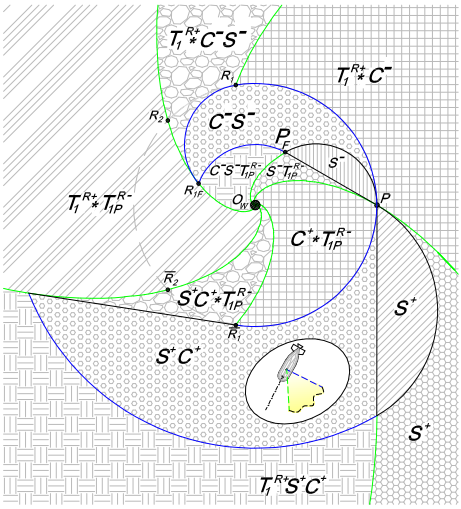

Figure 22: Partition of the motion plane for $\Gamma = \frac{\pi - \delta}{2}$, i.e. Borderline Side case (the left sensor border is aligned with the axle direction).

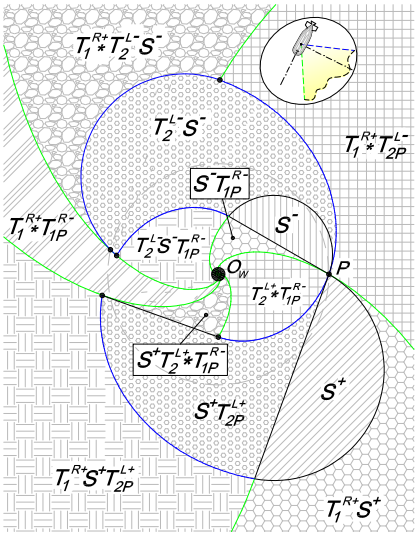

Figure 23: Partition of the motion plane for $\frac{\pi - \delta}{2} \leq \Gamma < \frac{\pi}{2}$, i.e. Asymmetric Lateral case (axle direction is included in the FOV).

Boyadzhiev, K. N. (1999). Spirals and conchospirals in the flight of insects. *The college mathematical journal*, 30(1):23–31.

Bryson, A. and Ho, Y. (1975). *Applied optimal control*. Wiley New York.

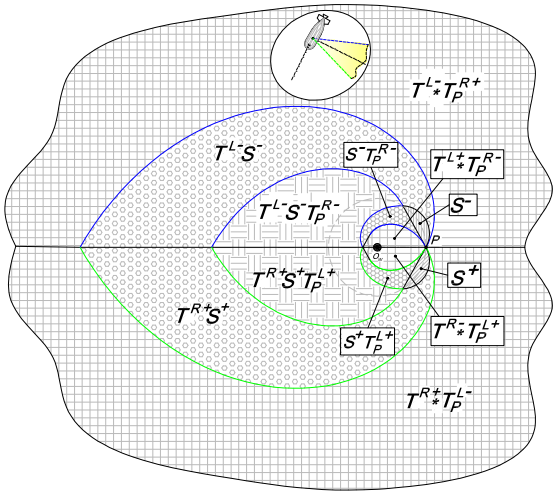

Figure 24: Partition of the motion plane for $\Gamma = \frac{\pi}{2}$, i.e. Symmetric Lateral case. In this case spiral have the same characteristic spiral, and hence $T_1 \equiv T_2 \equiv T$.

Bui, X., Souères, P., Boissonnat, J.-D., and Laumond, J.-P. (1994). Shortest path synthesis for Dubins non–holonomic robots. In *IEEE International Conference on Robotics and Automation*, pages 2–7.

Bullington, W. E. (1925). A study of spiral movement in the ciliate infusoria. *Arch. Protistenk*, 50:219 – 274.

Caprais, P. and Guyonic, S. (1997). Squint and forward looking synthetic aperture sonar. In *OCEANS '97. MTS/IEEE Conference Proceedings*, volume 2, pages 809 –814.

Cesari, L. (1983). Optimization-theory and applications: problems with ordinary differential equations. Springer-Verlag, New York.

Chitsaz, H., LaValle, S. M., Balkcom, D. J., and Mason, M. (2009). Minimum wheel-rotation paths for differential-drive mobile robots. *The International Journal of Robotics Research*, 28(1):66–80.

Dubins, L. E. (1957). On curves of minimal length with a constraint on average curvature, and with prescribed initial and terminal positions and tangents. *American Journal of Mathematics*, 79(3):457–516.

Dunkelberger, I. (1926). Spiral movement in mice. *Journal of Comparative Psychology (1921)*, 6(5):383 – 389.

Fraenkel, G. and Gunn, D. (1961). The orientation of animals. *Clarendon Press, 1940, reprinted Dover*.

Gans, N. and Hutchinson, S. (2007a). A stable vision-based control scheme for nonholonomic vehicles to keep a landmark in the field of view. In *Proc. IEEE Int. Conf. on Robotics and Automation*, pages 2196 –2201.

Gans, N. and Hutchinson, S. (2007b). Stable visual servoing through hybrid switched system control. *IEEE Transactions on Robotics*, 23(3):530–540.

Hayes, M. and Gough, P. (2009). Synthetic aperture sonar: A review of current status. *Oceanic Engineering, IEEE Journal of*, 34(3):207 –224.

Jean, F. (2008). Shadows, synthetic aperture sonar and forward looking gap-filler: different imaging algorithms. In *OCEANS 2008 - MTS/IEEE Kobe Techno-Ocean*, pages 1 –5.

Kawano, H., Kuwano, H., Irie, T., Maeda, H., Fukuda, Y., and Ikoma, N. (2009). Generation of panoramic image based on planar image features using side-view in-vehicle camera. In *ICCAS-SICE, 2009*, pages 4007 –4010.

Kleerekoper, H., Anderson, V. M., and Timms, A. M. (1973). Logarithmic spiral components in locomotor patterns of fish. *Canadian Journal of Zoology*, 51(3):397–400.

Langner, F., Knauer, C., Jans, W., and Ebert, A. (2009). Side scan sonar image resolution and automatic object detection, classification and identification. *in Proceeedings of OCEANS '09*.

Li, S. and Shimomura, Y. (2008). Lane marking detection by side fisheye camera. In *Intelligent Robots and Systems, 2008. IROS 2008. IEEE/RSJ International Conference on*, pages 606 –611.

López-Nicolás, G., Sagüés, C., Guerrero, J., Kragic, D., and Jensfelt, P. (2008). Switching visual control based on epipoles for mobile robots. *Robotics and Autonomous Systems*, 56(7):592 – 603.

Lyon, E. P. (1899). A contribution to the comparative physiology of compensatory motions. *American Journal of Physiology – Legacy Content*, 3:86–114.

Mariottini, G. L., Oriolo, G., and Prattichizzo, D. (2007). Image-based visual servoing for nonholonomic mobile robots using epipolar geometry. *Robotics, IEEE Transactions on*, 23(1):87 –100.

Mombaur, K., Truong, A., and Laumond, J.-P. (2010). From human to humanoid locomotion: an inverse optimal control approach. *Autonomous Robots*, 28:369–383.

Murrieri, P., Fontanelli, D., and Bicchi, A. (2004). A hybrid-control approach to the parking problem of a wheeled vehicle using limited view-angle visual feedback. *Int. Jour. of Robotics Research*, 23(4–5):437–448.

Ponda, S. S., Kolacinski, R. M., and Frazzoli, E. (2009). Trajectory optimization for target localization using small unmanned aerial vehicles. In *AIAA Guidance, Navigation, and Control Conference*, pages 1 – 25.

Pontryagin, L., Boltyanskii, V., Gamkrelidze, R., and Mishchenko, E. (1962). *The mathematical theory of optimal processes*. Interscience Publishers New York.

Reeds, J. A. and Shepp, L. A. (1990). Optimal paths for a car that goes both forwards and backwards. *Pacific Journal of Mathematics*, 145(2):367–393.

Rysdyk, R. (2003). Uav path following for constant line-of-sight. In *2nd AIAA "Unmanned Unlimited" Systems, Technologies, and Operations - Aerospace, Land, and Sea Conference, Workshop and Exhibition*.

Salama, A. I. A. and Hamza, M. H. (1978). Minimum time three dimensional interception. *Acta Astronautica*, 5:515–522.

Salaris, P., Fontanelli, D., Pallottino, L., and Bicchi, A. (2010). Shortest paths for a robot with nonholonomic and field-of-view constraints. *IEEE Transactions on Robotics*, 26(2):269–281.

Salaris, P., Pallottino, L., and Bicchi, A. (2011). Shortest paths with side sensors. In *Proc. IEEE Int. Conf. on Robotics and Automation*.

Schaeffer, A. A. (1920). On a new principle underlying movement in organisms. *Anat. Rec.*, 17:342 – 344.

Schaeffer, A. A. (1928). Spiral movement in man. *Journal of Morphology*, 45(1):293–398.

Souères, H. and Laumond, J. P. (1996). Shortest paths synthesis for a car-like robot. *IEEE Transaction on Automatic Control*, 41(5):672–688.

Sussmann, H. and Tang, G. (1991). Shortest paths for the reeds-shepp car: A worked out example of the use of geometric techniques in nonlinear optimal control. Technical report, Department of Mathematics, Rutgers University.

Theodorakopoulos, P. and Lacroix, S. (2008). A strategy for tracking a ground target with a uav. In *Intelligent Robots and Systems, 2008. IROS 2008. IEEE/RSJ International Conference on*, pages 1254 – 1259.

Tucker, V. A. (2000). The deep fovea, sideways vision and spiral flight paths in raptors. *The Journal of Experimental Biology*, 203:3745–3754.

Wang, H., Chan, Y., and Souères, P. (2009). A geometric algorithm to compute time-optimal trajectories for a bidirectional steered robot. *IEEE Transaction on Robotics*, (25)2:399-413.

Yu, J., LaValle, S., and Liberzon, D. (2012). Rendezvous without coordinates. *Automatic Control, IEEE Transactions on*, 57(2):421 – 434.

A Appendix

A.1 Proof of Theorem 1

Theorem 1. *Given two points $A = (\rho_A, \psi_A)$ and $B = (\rho_B, \psi_B)$, with $\psi_A > \psi_B$ and $\rho = \rho_A = \rho_B$, and an extremal path γ from A to B such that for each point G of γ, $\rho_G > \rho$, there exists an extremal path $\tilde{\gamma}$ from A to B such that for each point $\tilde{G}$ of $\tilde{\gamma}$, $\rho_{\tilde{G}} < \rho$ and $\ell(\tilde{\gamma}) < \ell(\gamma)$.*

Proof. Consider a point $Z = (\rho_Z, \psi_Z)$ such that $\rho_Z = \max_{G\in\gamma} \rho_G > \rho$. Let γ_1 and γ_2 the sub–paths of γ from Z to B and from Z to A.

The sub–path γ_1, is rotated and scaled (contracted of factor $\frac{\rho}{\rho_Z} < 1$) such that Z is transformed in A obtaining a path $\tilde{\gamma}_1$ from A to $\tilde{Z} = (\frac{\rho^2}{\rho_Z}, \psi_A + \psi_B - \psi_Z)$. Similarly, γ_2, can be rotated and scaled with the same scale factor but different rotation angle w.r.t. γ_1 such that Z is transformed in B, see figure 6. After geometrical considerations, it is easy to notice that the obtained path $\tilde{\gamma}_2$ starts in B and ends in $\tilde{Z}$.

The obtained paths are a contraction of γ_1 and γ_2 respectively and hence shorter. Moreover, any point G of γ_1 or γ_2 has $\rho_G > \rho$ hence is scaled in $\tilde{G}$ of $\tilde{\gamma}_1$ or $\tilde{\gamma}_2$ with $\rho_{\tilde{G}} = \frac{\rho\rho_G}{\rho_Z} < \rho$.

Concluding, we have obtained a shorter path from A to B that evolves completely in the disk of radius ρ. □

A.2 Proof of Theorem 2

Theorem 2. *Any path consisting in a sequence of a backward extremal arc followed by a forward extremal arc is not optimal.*

Proof. Observe that the distance from O_w is strictly increasing along backward extremal arcs (i.e. S^-, E_1^-, E_2^- with $E_2 \neq C$) and strictly decreasing along forward extremal arcs (i.e. S^+, E_1^+, E_2^+ with $E_2 \neq C$). For continuity of paths, for any sequence of a backward extremal followed by a forward one, there exist points A and B that verify hypothesis of Theorem 1, hence it is not optimal.

Any sequence consisting in an extremal S (or E_1) of length ℓ and an extremal $E_2 = C$ (in any order and direction) is inscribed in two circumferences centered in O_w. Hence, the shortest sequence is the one with $E_2 = C$ along the circle of smaller radius necessarily preceded by a forward S (or E_1) of same length ℓ.

Concluding, in an optimal path a forward arc cannot follow a backward arc. □

A.3 Proof of Theorem 3

Theorem 3. *Any path consisting in a sequence of an extremal arcs E_i and E_j followed in the same direction is not optimal for any $i, j \in \{1, 2\}$ with $i \neq j$.*

Proof. By proving the non–optimality of $E_i^+ * E_j^+$ the non–optimality of $E_j^- * E_i^-$ follows straightforwardly. Without loss of generality, we suppose $i = 1$ and $j = 2$. Let A and B be the initial and final points of the path γ of type $E_1^+ * E_2^+$ and N the intersection

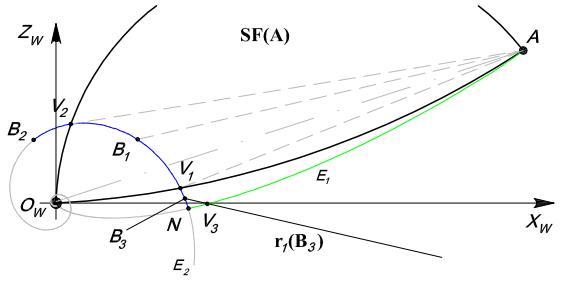

Figure 25: Construction of a path shorter than $E_1^+ * E_2^+$ for $0 \leq \Gamma \leq \frac{\delta}{2}$.

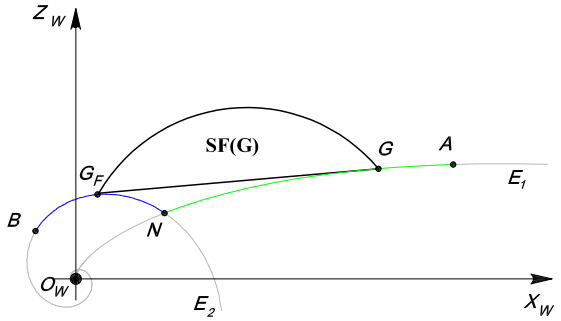

Figure 26: Construction of a path shorter than $E_1^+ * E_2^+$ for $\frac{\delta}{2} < \Gamma \leq \frac{\pi-\delta}{2}$.

points between E_1^+ and E_2^+. We now show for any value of Γ and δ there exists a sub–path of γ that can be shortened with a straight arc.

For $0 \leq \Gamma \leq \frac{\delta}{2}$, referring to figure 25, $SF(A)$ intersects the extremal E_2 in two points $V_1 \in \partial SF_1(A)$ and $V_2 \in \partial SF_2(A)$ and three cases occur: if $B \in SF(A)$, i.e. $B = B_1$ between V_1 and V_2 along E_2, γ is obviously longer than $\overline{AB}$; if $B = B_2$ is between V_2 and O_w, γ can be shortened by $\overline{AV_2}$; finally, if $B = B_3$ is between V_1 and N, considering $SB(B)$ and the intersection point V_3 between $\partial SB_1(B) = r_1(B)$ and E_1, γ can be shortened by $\overline{V_3 B}$.

For the Side case ($\frac{\delta}{2} < \Gamma < \frac{\pi-\delta}{2}$), there always exists a point G along E_1 between A and N such that $SF(G)$ intersects E_2 between N and B. Hence, γ can be shortened by $\overline{GG_F}$ (see figure 26). □

A.4 Proofs of Propositions 5, 6, 7, 8, and 9

To prove proposition 5, 6 and 7 and 9 the following technical result is needed.

Proposition 13. *Consider any two points G and H on a spiral arc E_i ($i = 1,2$). Let $\tilde{E}$ be the set of points between E_i and its symmetric w.r.t. $\overline{GH}$. A shortest path between G and H that evolves completely outside region $\tilde{E}$ is the arc of E_i between G and H.*

The proof of this proposition follows straightforwardly from the convexity property of $\tilde{E}$.

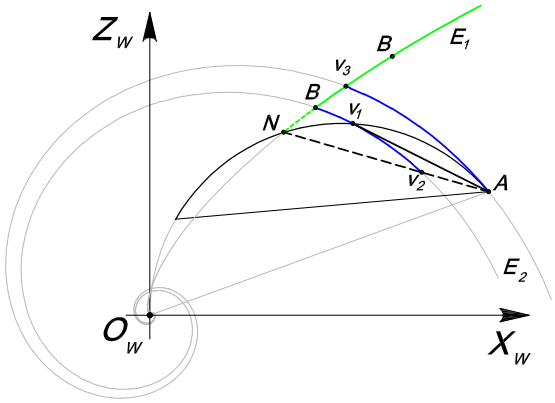

Figure 27: Construction used in the proof of Proposition 5 to short path $S^+ * E_1^-$.

Proposition 5. *From any starting point A, any path γ of type $S^+ * E_2^+$ ($S^- * E_1^-$) and $S^+ * E_1^-$ to B can be shortened by a path of type $S^+E_2^+$ ($S^-E_1^-$), S^+ (S^-) or $E_2^+ * E_1^-$.*

Proof. To be optimal, a path of type $S^+ * E_2^+$ ($S^- * E_1^-$) can be shortened by a path of type $S^+E_2^+$ ($S^-E_1^-$) or S^+ (S^-). Indeed, if $B \in SF(A)$ ($B \in SB(A)$), γ is shortened by $S^+ = \overline{AB}$ ($S^- = \overline{AB}$). However, let N be the intersection point between extremal arcs S^+ and E_2^+, from proposition 4 necessarily $N \in \partial SF_1(A) \cup \partial SF_2(A)$. In this case, for geometrical properties, S^+ and E_2^+ are tangent in N. Hence, path $S^+ * E_2^+$ is shortened by S^+ or $S^+E_2^+$. Equivalently, $S^- * E_1^-$ is shortened by S^- or $S^-E_1^-$.

Let now consider the path of type $S^+ * E_1^-$ and the non trivial case of $B \notin SF(A)$. From proposition 4, the intersection point N between S^+ and E_1^- must lay on $\partial SF_2(A)$. Considering now an arc $E_2(B)$ passing through B, two cases occur (see figure 27):

- if arc E_2 intersects $\partial SF_2(A)$ in V_1 and S^+ in V_2, by using Proposition 13, arc E_2 shortens path $S^+ * E_1^-$ between V_2 and B. A path from A to B of type $S^+ * E_2^+$ has been obtained, that in turn can be shortened by $S^+E_2^+$ through $V_1 \in \partial SF_2(A)$;
- otherwise, let us consider the arc E_2 through A. It intersects E_1 between B and O_w in V_3. By Proposition 13, the sub–path of γ between A and V_3 can be shortened by E_2. Hence, a shorter path of type $E_2^+ * E_1^-$ is has been obtained.

□

Proposition 6. *For $\frac{\delta}{2} \leq \Gamma \leq \frac{\pi}{2}$ (Side and Lateral cases), from any starting point A, any path γ of type $S^+ * E_1^+$ ($S^- * E_2^-$) or $S^+ * E_2^-$ can be shortened by a path of type S^+ (S^-), $E_1^+S^+$ ($E_2^-S^-$) or $E_1^+ * E_2^-$.*

Proof. If $B \in SF(A)$, γ is shortened by $S^+ = \overline{AB}$ ($S^- = \overline{AB}$). However, let us consider first a path γ of type $S^+ * E_1^+$ whose switching point $N \in \partial SF_1(A)$ for proposition 4. There always exists a straight line from B tangent to the extremal arc E_1 from A in V_1 between A and O_w. Let V_2 be the intersection point of this straight line and border

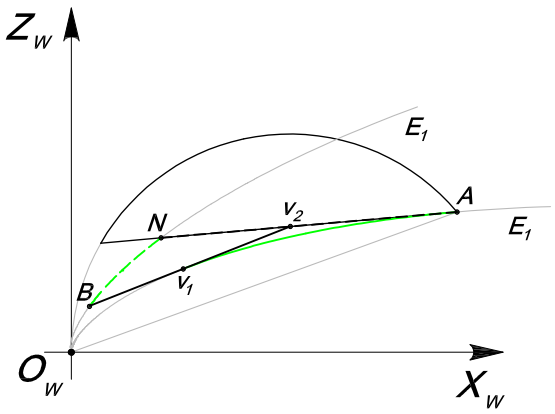

Figure 28: Construction used in the proof of Proposition 6 to short path $S^+ * E_1^+$.

$\partial SF_1(A)$ ($\partial SB_1(A)$). The unfeasible piecewise straight path from A to B through V_2 shortens path γ (see figure 28). In turn, the unfeasible polygonal path is longer than path $E_1^+ S^+$ through V_1. Equivalently $S^- * E_2^-$ can be shortened by $E_2^- S^-$.

For a path γ of type $S^+ * E_2^-$ whose switching point $N \in \partial SF_1(A)$ for proposition 4. Let us consider an extremal arc E_1 through B. Two cases can occur (see figure 29):

- if E_1 for A intersects arc E_2^- in V but B lays on E_2^- between V and O_w, by using the same construction of the unfeasible polygonal path above, γ can be shortened by $E_1^+ S^+$;
- otherwise the extremal V lays between B and O_w and for proposition 13, path of type $E_1^+ * E_2^-$ through V is shorter than $S^+ * E_2^-$.

□

Notice that, as an extension of proposition 4 for the Side and Lateral cases only, if an optimal path from Q to P includes a segment of type S^+ (or S^-) from G, then it ends on $\partial SF_2(G)$.

Proposition 7. *For $0 \leq \Gamma < \frac{\delta}{2}$ (Frontal case), from any starting point A, any path γ of type $S^+ * E_1^+$ or $S^+ * E_2^-$ can be shortened by a path of type S^+, $S^+ E_1^+$ or $E_1^+ * E_2^-$. Furthermore, for any path γ of type $S^- * E_2^-$ or $S^- * E_1^-$ can be shortened by a path of type S^-, $E_2^- S^-$ or $E_1^+ * E_2^-$.*

Proof. Any path γ of type $S^+ * E_1^+$ can be shortened by a path of type S^+ or $S^+ E_1^+$ for proposition 4. For paths $S^+ * E_2^-$ a similar procedure used for the path of type $S^+ * E_1^-$ in the second part of proof of proposition 5, can be followed. Proofs for paths $S^- * E_2^-$ or $S^- * E_1^-$ are equivalent to proof of proposition 6. □

Proposition 8. *For any starting point A, any path γ of type $S^+ * S^-$ can be shortened if the angle between arc S^+ and arc S^- is less than*

$$\psi_V \triangleq \phi_1 + \phi_2 + \frac{\sin(\phi_1+\phi_2)}{\cos\phi_1 \cos\phi_2}\left[2\ln\left(\frac{\sin(\phi_1+\phi_2)}{\cos\phi_1+\cos\phi_2}\right) + \ln\sin\phi_1 + \ln\sin\phi_2\right].$$

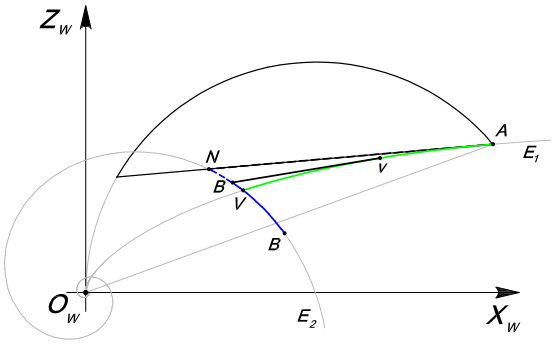

Figure 29: Construction used in the proof of Proposition 6 to short path $S^+ * E_2^-$.

Proof. The proof of this proposition follows straightforward from theorems 7 and 6; indeed they show that path $S^+ * S^-$ is optimal when the starting point Q lays on CS between V and P_S (see figure 13). □

Proposition 9. *For $\frac{\delta}{2} \leq \Gamma \leq \frac{\pi}{2}$ (Side and Lateral cases), $S^+ * S^-$ path can be shortened by paths of type $E_2^+ * S^-$, $S^+ * E_2^+$, $E_1^+ * S^+$ and $E_1^+ S^+$.*

Proof. The procedure used to prove this proposition is similar to that used in the proof of Proposition 5, 6 to short path $S^+ * E_1^-$ and $S^+ * E_1^+$ ($S^+ * E_2^+$), respectively. Constructions are similar to that shown in figure 27 replacing arc E_1^- with arc S^-, and in figure 28 (29) replacing arc E_1^+ (E_2^+) with arc S^+. □

A.5 Proof of Theorem 7

Theorem 7. *For any point $Q \in CS$, length L of a path $\gamma \in \mathscr{P}_Q$ (see figure 16) of type $T_1^{R+} * T_2^{R-} S^- T_1^{R-}$ is:*

- *for $0 \leq \alpha_{\overline{M}_1} \leq \phi_2 - \phi_1$, i.e. from P to P_F (notice that the last arc has zero length):*

$$L = \rho_P \left\{ \frac{\cos \alpha_{\overline{M}_1}}{\cos \phi_2} + \frac{1}{\cos \phi_1} + \right.$$
$$\left. - \frac{\cos \phi_1 + \cos \phi_2}{\cos \phi_1 \cos \phi_2} e^{\left(\psi_Q - \alpha_{\overline{M}_1}\right) \frac{t_1 t_2}{t_2 - t_1}} \left(\frac{\sin\left(\phi_2 - \alpha_{\overline{M}_1}\right)}{\sin \phi_2} \right)^{-\frac{t_1}{t_2 - t_1}} \right\}, \tag{16}$$

- *for $\alpha_{M_1} \geq \phi_2 - \phi_1$, i.e. from P_F to O_w:*

$$L = \rho_P \left\{ \frac{2}{\cos\phi_1} + e^{-\alpha_{M_1} t_1} \left[\frac{\cos(\phi_2 - \phi_1)}{\cos\phi_2} - \frac{1}{\cos\phi_1} + \right.\right.$$
$$\left.\left. - \frac{\cos\phi_1 + \cos\phi_2}{\cos\phi_1 \cos\phi_2} e^{[\psi_Q - (\phi_2 - \phi_1)] \frac{t_1 t_2}{t_2 - t_1}} \left(\frac{\sin\phi_1}{\sin\phi_2} \right)^{-\frac{t_1}{t_2 - t_1}} \right] \right\}, \tag{17}$$

with $t_1 = 1/\tan\phi_1$ *and* $t_2 = 1/\tan\phi_2$.

Proof. Recalling that $P = (\rho_P, 0)$, $Q = (\rho_P, \psi_Q)$, when $0 \leq \alpha_{\overline{M}_1} \leq \phi_2 - \phi_1$, $\overline{M}_1 \in \partial SF_2(P)$ (see proposition 4), by the law of sines we have

$$\rho_{\overline{M}_1} = \rho_P \frac{\sin(\phi_2 - \alpha_{\overline{M}_1})}{\sin\phi_2}, \tag{18}$$

and the length of segments S^- is

$$\overline{P\overline{M}}_1 = \rho_P \frac{\sin\alpha_{\overline{M}_1}}{\sin\phi_2}, \tag{19}$$

(cf. figure 16).

From (7), setting $t_2 = \frac{\cos\phi_2}{\sin\phi_2}$, the right logarithmic spiral passing through $\overline{M}_1$ (denoted with $T^R_{2\overline{M}_1}$) is given by

$$T^R_{2\overline{M}_1} : \left(\rho_{\overline{M}_1} e^{(\alpha_{\overline{M}_1} - \psi) t_2}, \psi \right).$$

Similarly, setting $t_1 = \frac{\cos\phi_1}{\sin\phi_1}$ the right spiral through Q (denoted as T^R_{1Q}) is given by

$$T^R_{1Q} : \left(\rho_Q e^{(\psi_Q - \psi) t_1}, \psi \right).$$

The intersection point between the spirals $T^R_{2\overline{M}_1}$ and T^R_{1Q} is $\overline{N} = (\rho_{\overline{N}}, \psi_{\overline{N}})$, where

$$\rho_{\overline{N}} = \rho_P \, e^{\left(\psi_Q - \alpha_{\overline{M}_1}\right) \frac{t_1 t_2}{t_2 - t_1}} \left(\frac{\sin\left(\phi_2 - \alpha_{\overline{M}_1}\right)}{\sin\phi_2} \right)^{-\frac{t_1}{t_2 - t_1}} \tag{20}$$

$$\psi_{\overline{N}} = \psi_Q \frac{t_1}{t_2 - t_1} - \alpha_{\overline{M}_1} \frac{t_2}{t_2 - t_1} - \frac{1}{t_2 - t_1} \ln \left(\frac{\sin\left(\phi_2 - \alpha_{\overline{M}_1}\right)}{\sin\phi_2} \right). \tag{21}$$

The length of the spiral arcs $T^R_{2\overline{M}_1}$ and T^R_{1Q} from $\overline{M}_1$ and Q to $\overline{N}$, respectively, are:

$$L_{\overline{M}_1 \overline{N}} = \frac{\rho_{\overline{M}_1} - \rho_{\overline{N}}}{\cos\phi_2},$$

$$L_{Q\overline{N}} = \frac{\rho_P - \rho_{\overline{N}}}{\cos\phi_1}\,.$$

Adding up, after some simplifications, the total length L is therefore as reported in (16).

When $\alpha_{M_1} \geq \phi_2 - \phi_1$, the optimal path is of type $T_1^{R+} * T_2^{R-} S^- T_1^{R-}$, where the last arc is a spiral arc passing through P, *i.e.* T_{1P}^{R-}. As a consequence, the switching point M_2 belongs to T_{1P}^{R-} (cf. figure 16). Moreover, from results of theorem 3 (see also figure 26), $M_1 \equiv M_{2F}$ and for simple geometrical considerations, $M_1 \in T_{1P_F}^R$. For this reasons, coordinates of point $M_2 = (\rho_{M_2}, \psi_{M_2})$ are

$$M_2 : \left(\rho_P\, e^{(\phi_2-\phi_1-\alpha_{M_1})t_1},\, \alpha_{M_1} - (\phi_2 - \phi_1)\right)\,, \tag{22}$$

and coordinates of point $M_1 = (\rho_{M_1}, \psi_{M_1})$ are

$$M_1 : \left(\rho_P \frac{\sin\phi_1}{\sin\phi_2}\, e^{(\phi_2-\phi_1-\alpha_{M_1})t_1},\, \alpha_{M_1}\right)\,. \tag{23}$$

The right logarithmic spiral $T_{2M_1}^R$ passing through M_1 is given by

$$T_{2M_1}^R : \left(\rho_{M_1}\, e^{(\alpha_{M_1}-\psi)t_2}, \psi\right)\,.$$

Similarly, the right logarithmic spiral through Q, denoted as T_{1Q}^R is given by

$$T_{1Q}^R : \left(\rho_P\, e^{(\psi_Q-\psi)t_1}, \psi\right)\,.$$

The intersection point between spirals T_{1Q}^R and $T_{2M_1}^R$ is point $N = (\rho_N, \psi_N)$, where

$$\rho_N = \rho_P\, e^{\psi_Q \frac{t_1 t_2}{t_2-t_1}}\, e^{-\alpha_{M_1} t_1}\, e^{-(\phi_2-\phi_1)\frac{t_1^2}{t_2-t_1}} \left(\frac{\sin\phi_1}{\sin\phi_2}\right)^{-\frac{t_1}{t_2-t_1}}\,, \tag{24}$$

$$\psi_N = \alpha_{M_1} + (\phi_2 - \phi_1)\frac{t_1}{t_2-t_1} - \psi_Q \frac{t_1}{t_2-t_1} + \frac{1}{t_2-t_1}\ln\left(\frac{\sin\phi_1}{\sin\phi_2}\right)\,. \tag{25}$$

The length of the arc of spiral T_{1P}^{R-} between P and M_2 is

$$L_{PM_2} = \frac{\rho_P - \rho_{M_2}}{\cos\phi_1} = \frac{\rho_P}{\cos\phi_1}\left(1 - e^{(\phi_2-\phi_1-\alpha_{M_1})t_1}\right)\,,$$

the length of arc S^- from M_1 to M_2 is

$$\overline{M_1M_2} = \rho_P \frac{\sin(\phi_2-\phi_1)}{\sin\phi_2}\, e^{(\phi_2-\phi_1-\alpha_{M_1})t_1}$$

and the length of the spiral arcs T_{1Q}^R and $T_{2M_1}^R$ from M_1 and Q to N, respectively, are

$$L_{M_1N} = \frac{\rho_P - \rho_N}{\cos\phi_1}\,,$$

$$L_{QN} = \frac{\rho_{M_1} - \rho_N}{\cos\phi_2}\,.$$

Adding up, after some simplifications, the total length L is obtained, as reported in (17). □